Chapter 1

Introduction

The term ‘nanometer’ refers to one billionth of a meter. The properties of the nanomaterials vary a great deal from that of the bulk material and their molecular state. This is mainly due to i) an increase in the surface/volume ratio when we decrease the dimension of the material to nanometer scale and ii) quantum confinement of nanomaterials, which changes the energy band structure of the material and in turn modifies the electronic properties of the materials [1]. This size dependency reflects in many properties of nanoscale materials such as optical properties, magnetic properties, melting points, specific heats and surface reactivities etc [2]. Nanotechnology is the application of these nanostructured materials to form useful nanoscale devices [3].

1.1 Nanoparticles

Nanoparticles, an important class of nanoscale materials have a wide range of applications. The definition of a nanoparticle can be given as “A particle having all the dimensions of the order of 100 nm or less” [4]. Metal nanoparticles have potential applications in heterogeneous catalysis [5], bio-medicine [6] and magnetic data storage [7]. Metal nanoparticles exhibit interesting optical properties at the nanoscale because of ‘surface plasmon resonance’ and have preferential applications as photonic crystals [8]. Metal nanoparticles exhibit good catalytic properties because a large portion of metal atoms are at the surface and available for catalysis. Gold, platinum and palladium nanoparticles are some of the metals currently used for catalysis [9]. Bimetallic nanoparticles, composed of two different metal elements have unique catalytic, optical, electronic and magnetic properties distinct from their corresponding monometallic nanoparticles. Two main groups of bimetallic

nanoparticles exist; namely, alloys and layered (core-shell) nanoparticles. Bimetallic alloy nanoparticles have potential applications in catalysis because of their higher activity than the corresponding monometallic nanoparticles. This is due to the change in the electron structure of the metal nanoparticle or the change in its morphology due to the addition of second material [10]. The magnetic properties of the monometallic nanoparticles can be significantly enhanced by formation of alloys, which provide high magnetic anisotropy and high coercivities making them preferential candidates for ultra high density magnetic recording [11]. All the unique properties of bimetallic nanoparticles such as tuning of surface plasmon energy band, improved catalytic properties and magnetic properties are sensitive to size, composition and compositional distribution, which depend upon the technique used to produce the nanoparticles.

1.2 Nanoparticle synthesis

The synthesis of monodisperse nanoparticles is of great scientific and technological importance. Controlling the size and shape of nanoparticles is crucial to exploit their novel properties. Hence there is a need for methods to synthesize nanoparticles of desired size and shape. The synthesis routes can be classified into two categories, namely, vapor phase and solution phase synthesis.

Vapor phase synthesis involves creation of supersaturated vapor containing the solid material to be prepared in nanoparticulate form, leading to homogeneous nucleation followed by subsequent condensation and coagulation of monomers [12]. The vapor phase synthesis methods can be classified based on the source and the type of energy used to create supersaturation. Inert gas condensation, pulsed laser ablation, spark discharge generation and ion sputtering are the methods that use a solid precursor to generate metal atoms. Chemical vapor synthesis, spray pyrolysis and thermal plasma synthesis etc. uses liquid or vapor phase precursors to induce supersaturation in gas phase [13]. Absence of hazardous chemicals and good control over particle size and size distribution are the main advantages, whereas

inhomogeneous temperature distributions and vortex formation are some of the disadvantages of vapor phase synthesis routes [12].

Solution phase synthesis involves a chemical reaction to generate metal atoms by reduction of a metal precursor. Sonomechanical, sonochemical, polyol reduction, and synthesis in microemulsions etc. are some of the solution phase synthesis methods employed to generate nanoparticles. Microemulsion based synthesis has attracted lot of attention as nanoparticles can be synthesized at room temperature with good control over size and size distribution.

1.3 Project objectives

The main objective of any nanoparticle synthesis method is to achieve control over particle size and polydispersity. The first part of this project is a follow-up on the work done by Girish [14]. Girish synthesized gold nanoparticles in water/AOT/Brij-30/isooctane mixed microemulsions and studied the effect of reagent concentrations, co-surfactant concentration, temperature and addition rate of reducing agent on size and stability of gold nanoparticles synthesized. It was found that the mean size and polydispersity decrease with an increase in rate of addition of hydrazine. The amount of reducing agent needed to form stable particles was found to be 12 times in excess of the stoichiometric requirement, which was attributed to the possibility of a side reaction between hydrazine and AOT. Gold nanoparticles synthesized at low addition rates of reducing agent were not as stable as the particles synthesized at higher addition rates of reducing agent. The observed effect of hydrazine addition rate on the mean size of gold nanoparticles at different temperature is shown in Figure 1.1 [14].

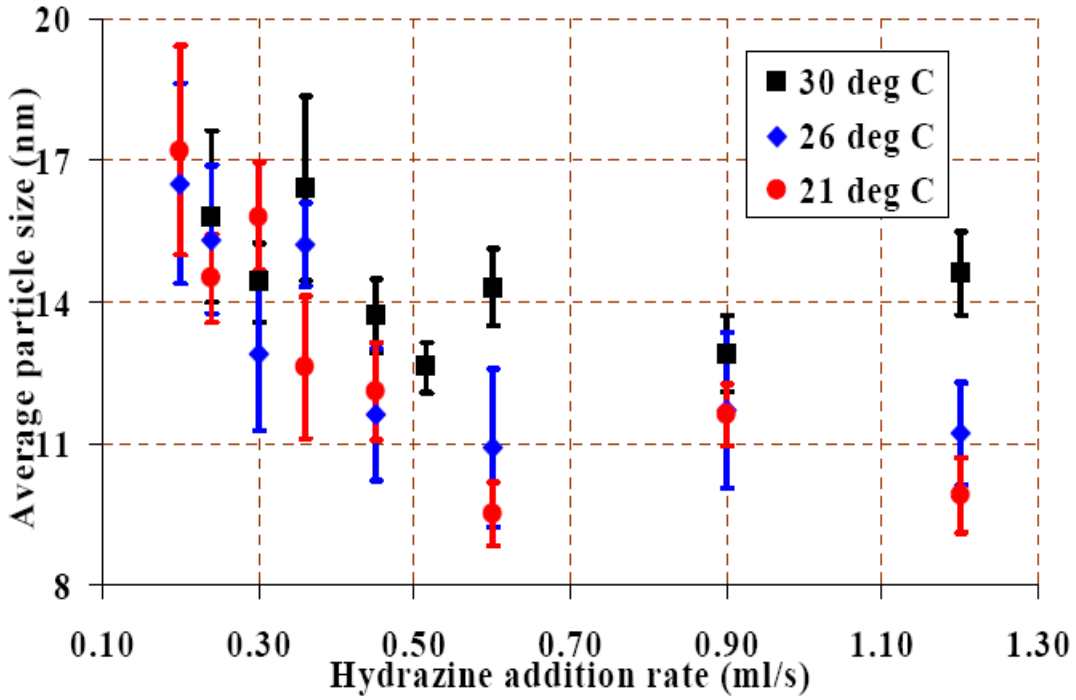

Figure 1.1: Effect of hydrazine addition rate on the mean size of the gold nanoparticles synthesized in water/AOT/Brij-30/isooctane mixed microemulsions at different temperatures. Reproduced from [14].

The preliminary experiments done in this study is based on the final results obtained by Girish [14]. In his experimental setup, a plastic tube is used to inject reducing agent hydrazine hydrate microemulsion into gold chloride microemulsion at different flow rates. When he replaced the old tube by a new tube, he observed a peak in the UV-Visible absorption spectrum of the final nanoparticle solution, shown by an oval boundary in Figure 1.2.

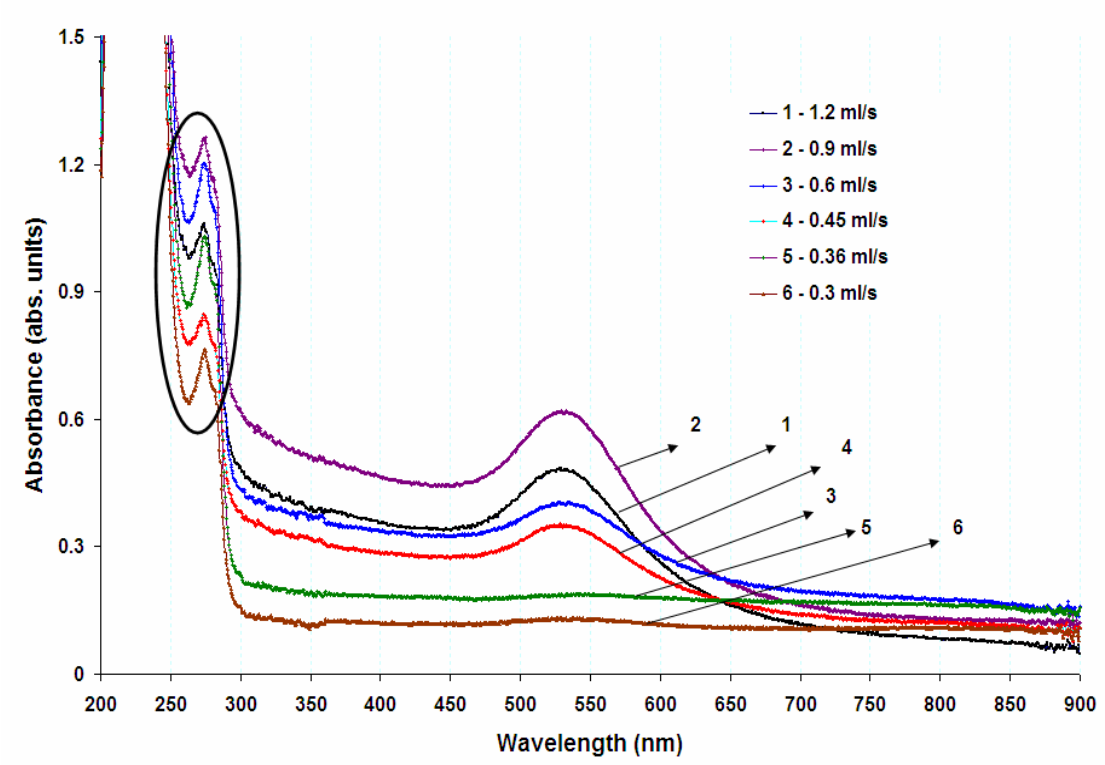

Figure 1.2: UV-Visible spectra of gold nanoparticle solutions synthesized with a new PVC tube at different addition rates of reducing agent. Synthesis conditions: [$HAuCl_4$]: 0.075 M; [N_2H_5OH]: 0.75 M; [AOT]: 0.2 M; [$C_{12}E_4$]: 0.2 M; [water]/ [AOT]: 8; The oval region indicates a peak at 274 nm that is attributed to the presence of unreacted gold chloride [14].

The peak at 274 nm represents unreacted gold chloride. This is unexpected because the reducing agent used was twelve times in excess of the stoichiometric requirement. The immediate objective was to understand and overcome these issues of unreacted gold chloride and the need for an excess of reducing agent. The overall objective was to understand the effect of reagent addition rate on the size and stability of nanoparticles synthesized in microemulsions. A further objective of this project was to develop a standard protocol for synthesizing bimetallic alloy nanoparticles, in particular FePt nanoparticles in microemulsions, which are suitable for technological applications.

This report has been organized in the following order. Chapter 2 reviews the synthesis methods published in literature to produce bimetallic and FePt alloy nanoparticles. Chapter 3 gives an overview of microemulsions and synthesis of nanoparticles in microemulsions. Chapter 4 explains the experimental protocol and discusses the various nanoparticle characterization techniques that have been used. Chapter 5 focuses on the experiments performed to understand the effect of excess hydrazine and pH on the stability of gold nanoparticle dispersion along with the study of effect of addition rate on particle size. In Chapter 6, preliminary experiments carried out to synthesize FePt nanoparticles are presented. Chapter 7 summarizes the work done followed by recommendations for future work.

1.4 References

1. K. J. Klabunde, 'Nanoscale Materials in Chemistry', A John Wiley & Sons, Inc., Publication, 2001.
2. http://en.wikipedia.org/wiki/Nanomaterials, accessed on 22/01/07.
3. M. Ratner and D. Ratner, Nanotechnology, 'A Gentle Introduction to the Next big Idea', Pearson Publications, 2005.
4. http://www.nanocompositech.com/glossary-nanocomposite-nanotechnology.htm, accessed on 18/01/07.
5. B. F. G. Johnson, 'Nanoparticles in Catalysis' *Topics in Catalysis*, 24, 2003, 1-4.
6. P. K. Jain, I. H. El-Sayed and M. A. El-Sayed, 'Au nanoparticles target cancer' *Nano Today*, 2, 2007, 18-29.
7. S. Sun, 'Recent Advances in Chemical Synthesis, Self-Assembly and Applications of FePt Nanoparticles' *Advanced Materials,* 18, 2006, 393–403.
8. P. A. Rundquist, P. Photinos, S. Jagannathan, and S. A. Asher, 'Dynamic Bragg diffraction from crystalline colloidal arrays' *Journal of Chemical Physics* 91, 1989, 4932-4941.

9. Q. wang, A. E. Ostafin, 'Metal Nanoparticles in Catalysis', *Encyclopedia of Nanoscience and Nanotechnology*, 5, 2004, 475-503.
10. D. I. Gracia-Gutierrez, C. E. Gutirrez-Wing, L. Giovanetti, J. M. Ramallo-Lopez, F. G. Requezo, and M. Jose-Yacaman, 'HAADF study of Au-Pt core-shell bimetallic nanoparticle' *Applied Physics A,* 79, 2004, 481-487.
11. X. Du, M. Inokuchi, and N. Toshima, 'Preparation and characterization of Co-Pt bimetallic magnetic nanoparticles' *Journal of Magnetism and Magnetic Materials*, 299, 2006, 21-28.
12. C. Baker, A. Pradhan, and S. I. Shah, 'Metal Nanoparticles', *Encyclopedia of Nanoscience and Nanotechnology*, 5, 2004, 449-473.
13. M. T. Swihart, 'Vapor phase synthesis of nanoparticles', *Current Opinion in Colloid and Interface Science,* 8, 2003, 127-133.
14. M. Girish, 'Nanoparticle synthesis in microemulsions', Master of Engineering Report, *Indian Institute of Science,* 2007.

Chapter 2

Literature Review

2.1 Bimetallic nanoparticles

Bimetallic nanoparticles, composed of two different elements have unique catalytic, optical, electronic and magnetic properties distinct from their corresponding monometallic nanoparticles. The chemical and physical properties of bimetallic nanoparticles depend not only on size and composition but also on whether the particle is a core/shell particle or an alloyed one. All the unique properties of bimetallic nanoparticles such as tuning of surface plasmon energy band, improved catalytic properties and magnetic properties are sensitive to size, composition and compositional distribution, which depend upon the protocol used to produce the nanoparticles. Hence developing a synthesis protocol to effectively control the size and compositional distribution is crucial for practical applications.

2.2 Synthesis of bimetallic nanoparticles

Bimetallic nanoparticles are generally synthesized in i) Gas phase synthesis and ii) solution based processes.

Gas phase synthesis techniques mainly depend on vaporization or sputtering to generate metal atoms, which subsequently undergo nucleation and growth to form nanoparticles. The laser vaporization controlled condensation (LVCC) and DC Magnetron sputtering are two typical synthesis techniques of gas phase processes [1]. Though gas phase synthesis techniques produce nanoparticles free of contamination, the size distribution of the particles is broad and controlling the composition of nanoparticles becomes complicated apart from the high cost of the equipment used [1].

Bimetallic nanoparticles can be prepared in solution either by i) simultaneous reduction (co-reduction) of two metal ions or ii) sequential reduction of one metal salt in the presence of the nuclei of another with or without a protective agent. Core/shell bimetallic nanoparticles are usually synthesized by the second method. The main strategies used to prepare bimetallic nanoparticles include polyol reduction [2, 3], citrate reduction [4], sonochemical method [5, 6] and reverse micellar route [7].

Using a diol or polyalcohol to reduce metal salts to form metal nanoparticles is called polyol process. Both alloy and core/shell nanoparticles can be produced by this method. Liu et al. have synthesized monodisperse FePt nanoparticles by simultaneous reduction of iron acetylacetonate and platinum acetylacetonate using 1,2-hexadecanediol as a reducing agent at 286^0 C [2]. As prepared FePt nanoparticles were 3 nm in diameter with a standard deviation of 10%. Oleic acid and oleyl amine were used as stabilizers for inhibiting particle aggregation. Final nanoparticle composition was controlled by adjusting the initial concentrations of metal precursors. Core/shell nanoparticles were also synthesized using modified polyol process at 205^0 C [3]. Monodisperse Pt nanoparticles were prepared first and used as seeds upon which cobalt shell was formed by thermal decomposition of cobalt carbonyl. The thickness of the cobalt shell was controlled by adjusting the initial concentration of cobalt carbonyl compound. The decomposition of cobalt carbonyl was performed at low temperature to avoid alloy formation.

Gold-silver alloy nanoparticles were synthesized in aqueous medium by co-reduction of chlorauric acid and silver nitrate with sodium citrate [4]. This method was a variation of the method developed by Turkevich [8]. The optical absorption spectrum showed a single absorption peak, which indicates the presence of alloy particles and the maximum of plasmon absorption band was found to vary linearly with the mole fraction of gold.

In sonochemical method, ultrasonic sound at high frequency was used to reduce the metals salts. Vinodgopal et al. have synthesized Pt-Ru core-shell nanoparticles by successive reduction of metal precursors in aqueous solution by

ultrasonic irradiation [5]. The ultrasonic wave creates cavitation in the solution, which will generate highly reactive $H^{\cdot}$ and $OH^{\cdot}$ radicals. These radicals reduce the metal salts either directly or by forming other type of radicals by reacting with organic solvents, which then reduce the metal salts. The average diameter of the platinum particles obtained was 5 nm and these are coated with a ruthenium shell, which increased the average particle size to 15 nm. Bimetallic gold/palladium core/shell nanoparticles were also produced in aqueous solution by this method [6]. In both cases sodium dodecyl sulphate (SDS) was used to stabilize the particles.

Weihua et al. synthesized platinum-copper (Pt-Cu) bimetallic alloy nanoparticles in water/CTAB/n-butanol/isooctane microemulsions [7]. The final nanoparticle composition was observed to be similar to the initial precursor ratios. Gold-platinum (Au-Pt) bimetallic nanoparticles of average size 3-4.5 nm were synthesized by using water/AOT/Isooctane microemulsions using hydrazine as a reducing agent [9]. The initial precursor molar concentration was varied from 9:1 to 1:9 and the final composition of the nanoparticles was observed to be similar to the ratio of the precursor molar concentration in feed. Similarly platinum-silver (Pt-Ag) [21], silver-gold (Ag-Au) [22], palladium-platinum (Pd-Pt) [23], copper-nickel (Cu-Ni) [24] bimetallic nanoparticles have also been synthesized. TEM images have shown that particles were essentially alloys composed of both metals uniformly distributed in the particle.

2.3 Synthesis of FePt nanoparticles

FePt nanoparticles have gained attention over the last decade as they have potential applications in ultra high density magnetic data storage. The coercivity or the magnetic anisotropy energy is an important property, which determines the stability of the magnetization in bulk material as well as in nanoparticles. This coercive force should be higher for the materials to be useful in high density magnetic data storage. This coercivity depends on various factors such as size (for metals), composition (for alloys) and various forms of anisotropy. Face centered

tetragonal (FCT) structured FePt alloys have large magnetocrystalline anisotropy (K_u = 6.6-10 × 10^6 J/m^3) and good chemical stability [14], which is an essential criterion for storage applications.

There are several methods to synthesize FePt nanoparticles, which include vacuum deposition techniques, polyol reduction, modified polyol process (two step approach) and reverse micellar synthesis.

In vacuum deposition techniques, FePt thin films were deposited by DC magnetron sputtering of elemental Fe and Pt targets onto a substrate using argon [15]. The as prepared films have disordered face centered cubic structure (FCC) and annealing is needed to convert the FCC structure to FCT structure. Controlling the composition of the nanoparticle thin film is an issue in this process.

FePt nanoparticles were also synthesized by polyol reduction of platinum acetylacetonate, $Pt(acac)_2$ and thermal decomposition of iron penta carbonyl, $Fe(CO)_5$ simultaneously at a high temperature of 297^0 C [16]. The as formed FePt nanoparticles were monodisperse ($\sigma < 5\%$), 4 nm in diameter and stabilized by oleic acid and oleyl amine. The final nanoparticle composition was different from the initial metal precursor ratio. This is due to slow decomposition of $Fe(CO)_5$ caused by the formation of the $Fe(CO)_5$ vapor phase at the reaction temperature. The FePt nanoparticle assemblies were annealed at 600^0C to convert the particle structure from FCC to FCT. The recording experiments were performed on FePt nanoparticle assembly and the read/write signals obtained indicated that FePt nanoparticles can be used for magnetic recording applications.

In order to avoid the hazardous effects of $Fe(CO)_5$ and to obtain effective control of composition, an iron salt ($Fe(acac)_2$, $FeCl_2$) was used in place of $Fe(CO)_5$ and both iron and platinum salts were reduced with a polyol [2]. FePt nanoparticles obtained by this method have a mean diameter of 2-3 nm and exhibit FCC structure. The advantage of this method over the previous method is control of composition. Initial feed composition is retained in the final nanoparticles. There are several modifications to this procedure to produce partial FCT structured FePt nanoparticles by using high boiling point solvents like tetraethylene glycol, hexadecylamine [17],

and to reduce the transition temperature by adding Cu, Pb, or Sn [18]. Avoiding particle agglomeration during high temperature annealing is critical for technological applications and so, forming FePt nanoparticles in an inert matrix like silica, or organic linker molecules were attempted and they were found to be successful in avoiding particle agglomeration [19].

FePt nanoparticles were also synthesized by relatively low temperature methods like aqueous phase reduction and reverse micellar synthesis. In aqueous phase, both iron and platinum salts were simultaneously reduced with a powerful reducing agent (hydrazine) in the presence of surfactants SDS and CTAB leading to the formation of FePt alloy nanoparticles [20]. It was observed that the addition of copper to the system reduced the coalescence of particles.

Carpenter et al. have synthesized FePt nanoparticles in water in oil (w/o) microemulsions formed by cationic surfactant CTAB and co-surfactant 1-butanol in octane at a water/CTAB molar ratio of eight [21]. Metal salts were reduced simultaneously by using sodium borohydride, which was added directly to the microemulsion. They were able to synthesize both FePt and $FePt_3$ nanoparticles by controlling the initial precursor ratio. The average size of the $FePt_3$ nanoparticles obtained from transmission electron microscope (TEM) was 10 nm and the particles were found to be superparamagnetic at room temperature. Nonionic surfactants like brij-52 and brij-56 were also used to produce FePt nanoparticles [22]. Different water/surfactant ratios were used and they were able to synthesize monodisperse particles (COV = 8-11 %) of size ranging from 4.5 nm to 20 nm. Particles were capped with octadecanethiol to prevent agglomeration. Final nanoparticle composition was found to be nearly the same (difference < 4%) as that of the feed composition. Results from X-ray diffraction (XRD) and high resolution TEM have shown the presence of smaller crystalline domains in nanoparticles. The as prepared nanoparticles were superparamagnetic and annealing was done to achieve FCT structure. FePt nanoparticles were coated with a silica shell to prevent agglomeration during the annealing process and the silica shell was functionalized with organosilane molecules to make the particles dispersible in nonpolar solvents for forming ordered

arrays of nanoparticles. Presence of silica shell effectively hindered the agglomeration of nanoparticles and the magnetic properties of the particles were not affected.

Since coercivity depends on both nanoparticle composition and size, it is necessary to use or develop a method by which both these parameters can be controlled. Both size and composition can be effectively controlled in microemulsions making this method an attractive procedure to synthesize FePt nanoparticles required for ultra high density recording.

2.4 Conclusions

This chapter reviewed different synthesis protocols available for synthesizing bimetallic nanoparticles and FePt nanoparticles. FePt nanoparticles are potential candidates for ultra high density magnetic media and biomedical applications. Using microemulsions, FePt nanoparticles can be synthesized at room temperature with good control over size and composition.

2.5 References

1. V. Abdelsayed, K. M. Saoud and M. Samy El-Shall, 'Vapor phase synthesis and characterization of bimetallic alloy and supported nanoparticle catalysts' *Journal of Nanoparticle Research,* 8, 2006, 519-531.
2. C. Liu, X. Wu, T. Klemmer, N. Shukla, X. Yang, D. Weller, A. G. Roy, M. Tanase, and D. Laughlin, 'Polyol Process Synthesis of Monodispersed FePt Nanoparticles' *Journal of Physical Chemistry B,* 108, 2004, 6121-6123.
3. N. S. Sobal, U. Ebels, H. Mohwald, and M. Giersig, 'Synthesis of Core-Shell PtCo Nanocrystals' *Journal of Physical Chemistry B,* 107, 2003, 7351-7354.

4. S. Link, Z. L. Wang, and M. A. El-Sayed, 'Alloy Formation of Gold-Silver Nanoparticles and the Dependence of the Plasmon Absorption on Their Composition' *Journal of Physical Chemistry B,* 103, 1999, 3529-3533.
5. K. Vinodgopal, Y. He, M. Ashokkumar, and F. Grieser, 'Sonochemically Prepred Platinum-Rutenium Bimetallic Nanoparticles' *Journal of Physical Chemistry B,* 110, 2006, 3849-3852.
6. Y. Mizukoshi, K. Okitsu, Y. Maeda, T. A. Yamamoto, R. Oshima, and Y. Nagata, 'Sonochemical Preparation of Bimetallic Nanoparticles of Gold/Palladum in Aqueous Solution' *Journal of Physical Chemistry B,* 101, 1997, 7033-7037.
7. W. Weihua, T. Zuelin, C. Kai, and C. Gengyu, 'Synthesis and characterization of Pt-Cu bimetallic alloy nanoparticles by reverse micelles method' *Colloids and Surfaces A: Physicochemical Engineering Aspects,* 273, 2006, 35-42.
8. J. Turkevich, P. C. Stevenson, J. Hiller, 'A Study of the Nucleation and Growth Processes in the Synthesis of Colloidal Gold' *Discussions of the Faraday Society***,** 11, 1951, 55-75.
9. M. Wu, D. H. Chen, and T. C. Huang, 'Preparation of Au/pt Bimetallic Nanoparticles in Water-in-Oil Microemulsions' *Chemistry of Materials,* 13, 2001, 599-606.
10. M. Li Wu, L. Biao Lai, 'synthesis of Pt/Ag bimetallic nanoparticles in water-in-oil microemulsions' *Colloids and Surfaces A: Physicochemical Engineering Aspects,* 244, 2004, 149-157.
11. A. Pal, S. Shah, and S. Devi, 'Preparation of silver, gold and silver-gold bimetallic nanoparticles in w/o microemulsion containing TritonX-100' *Colloids and Surfaces A: Physicochemical Engineering Aspects,* 302, 2007, 483-487.
12. M. Li Wu, D. Hwang Chen, and T. Chia Huang, 'Preparation of Pd/Pt Bimetallic Nanoparticles in Water/AOT/Isooctane Microemulsions' *Journal of Colloid and Interface Science* 243*,* 2001, 1002-1008.

13. J. Feng, C. Ping Zhang, 'Preparation of Cu-Ni alloy nanocrystallitees in water-in-oil microemulsions' *Journal of Colloid and Interface Science,* 293, 2006, 414-420.

14. D. Weller, A. Moser, L. Folks, M. E. Best, W. Lee, M. F. Toney, M. Schwickert, J. U. Thiele, and M. F. Doerner, 'High Ku Materials Approach to 100Gbits/in^2' *IEEE Transactions on Magnetics,* 36, 2000, 10-15.

15. K. R. Coffey, M. A. Parker and J. K. Howard, 'High Anisotropy $L1_0$ Thin Films for Longitudinal Recording' *IEEE Transactions on Magnetics*, 31, 1995, 2737-2739.

16. S. Sun, C. B. Murray, D. Weller, L. Folks, and A. Moser, 'Monodisperse FePt Nanoparticles and Ferromagnetic FePt Nanocrystal superlattices' *Science,* 287, 2000, 1989-1992.

17. S. Sun, 'Recent Advances in Chemical Synthesis, Self-Assembly and Applications of FePt Nanoparticles' *Advanced Materials*, 18, 2006, 393-403.

18. B. Jeyadevan, A. Hobo, K. Urakawa, C. N. Chinnasamy, K. Shinoda, and K. Tohji, 'Towards direct synthesis of fct-Fept nanoparticles by chemical route' *Journal of Applied Physics,* 93, 2003, 7574-7576.

19. Y. Tamada, S. Yamamoto, M. Takano, S. Nasu, and T. Ono, 'Well-ordered $L1_0$-FePt nanoparticles synthesized by improved SiO_2-nanoreactor method' *Applied Physics Letters,* 90, 2007, 1625091-1625093.

20. P.Gibot, E. Tronc, C. Chaneac, J.P. Jolivet, D. Fiorani, and A.M. Testa, '(Co,Fe)Pt nanoparticles by aqueous route; self-assembling, thermal and magnetic properties' *Journal of Magnetism and Magnetic Materials,* 290-291, 2005, 555-558.

21. E. E. Carpenter, J. A. Sims, J. A. Wienmann, W. L. Zhou, and C. J. O'Connor, 'Magnetic properties of iron and iron platinum alloys synthesized via microemulsion techniques' *Journal of Applied Physics,* 87, 2000, 5615-5617.

22. Q. Yan, A. Purkayastha, T. Kim, R. Kroger, A. Bose, and G. Ramanath, 'Synthesis and Assembly of Monodisperse High-Coercivity Silica-Capped FePt Nanomagnets of Tunable Size, Composition, and Thermal Stability from Microemulsions' *Advanced Materials,* 18, 2006, 2569-2573.

Chapter 3

Microemulsions: An Overview

A microemulsion can be defined as "a system of water, oil and an amphiphile, which is a single optically isotropic and thermodynamically stable liquid solution" [1]. The term microemulsion was first used by Schulman et al. [2] in 1959. It was Schulman et al. who noticed that coarse macroemulsions stabilized by an ionic surfactant became transparent after addition of a medium chain length alcohol. Ordinary emulsions are thermodynamically unstable and their formation requires input of energy, whereas microemulsions form spontaneously since they are thermodynamically stable. The stability is due to the presence of fairly large amount of surfactants. A variety of surfactants have been used to form microemulsions. These include common soaps, ionic and nonionic surfactants. Microemulsions are also called as micellar emulsions and swollen micelles in literature. This chapter gives a brief overview of microemulsions and synthesis of nanoparticles in microemulsions.

3.1 Microemulsions

Microemulsions are thermodynamically stable and optically transparent dispersions of oil and water stabilized by surfactants. Microemulsions contain huge oil/water interfacial areas. Due to the presence of surfactant molecules, interfacial tension is very low, usually << 1 mN/m [3]. These very low interfacial tensions are crucial for the formation of microemulsions and depend on system composition.

As the concentration of surfactant exceeds their critical micellar concentration (CMC), self assembled aggregates called micelles or reverse micelles are formed. These reverse micelles (or micelles), upon addition of water (or oil) swell and hence are called as swollen (reverse) micelles or (reverse) microemulsions. Microemulsions

are of two types, namely oil in water microemulsions and water in oil (reverse) microemulsions. For water in oil microemulsions, the hydrodynamic radius of the droplet is dependent on water content [4]. The typical size of these droplets is below the wavelength of visible light and hence these microemulsions appear optically clear.

The Surfactants used are characterized by the presence of hydrophobic and hydrophilic parts. The hydrophobic part usually is a long and flexible hydrocarbon chain, whereas the hydrophilic part is formed by a polar or an ionic head group. Depending on the nature of the head group, surfactants are distinguished as nonionics (e.g. Polyoxyethylene (4) lauryl ether, Brij 30), cationic (e.g. Cetyltrimethylammonium bromide), anionic (e.g. Dioctylsulfosuccinate, AOT) and zwitterionics (e.g. Dipalmitoylphosphatidylcholine).

3.2 Packing parameter

It has been found out that the preferred structure of surfactant aggregates is determined by a geometrical parameter called the critical packing parameter (CPP), which is defined as $v/(a_0 * l_c)$. Where, v is the volume of the surfactant alkyl chain, a_0 is the head group area and l_c is the length of the fully extended alkyl chain [5]. Based on geometric consideration, it was found out that if CPP < 1/3, then that surfactant is suitable to form spherical micelles. If CPP is in between 1/3 and 1/2, the preferred structures are cylindrical micelles and if CPP is between 1/2 and 1, the preferred structures are lamellar phases and bilayers. If CPP >1, then reverse micelles will be formed.

3.3 Hydrophilic-Lipophilic Balance (HLB)

Apart from CPP, another parameter that effects surfactant self assembly is their ability to interact with aqueous and organic media. This property is defined by

hydrophilic-lipophilic balance (HLB). The possibility of forming a microemulsion depends strongly on the balance between surfactant's hydrophilic and lipophilic properties, determined not only by surfactant structure but also by other factors such as temperature, salinity etc [6]. HLB is generally expressed as an empirical equation based on the relative proportions of hydrophobic and hydrophilic groups within the molecule. Lower HLB values result in reverse micelles where as higher HLB values result in micelles and intermediate HLB values result in bilayers, vesicles etc.

3.4 Droplet Kinetics

In solution, microemulsion droplets are in a continuous random (Brownian) motion, which results in collision of droplets, formation of transient dimers and their breakdown. The typical life time of transient clusters is in the order of microseconds [5]. Internal contents of the droplets are known to exchange, typically on millisecond time scale depending on the droplet concentration [7]. A possible mechanism could be the collision of droplets and transient merging of droplet cores during which the contents are exchanged. Droplet exchange depends on film flexibility, which is greatly effected by the presence of co-surfactants [8].

3.5 Synthesis of nanoparticles in microemulsions

Microemulsion droplets have the ideal environment to synthesize nanoparticles since nucleation and growth takes place inside the droplets stabilized by surfactants. A schematic illustration of nanoparticle formation in microemulsions is given in Figure 3.1.

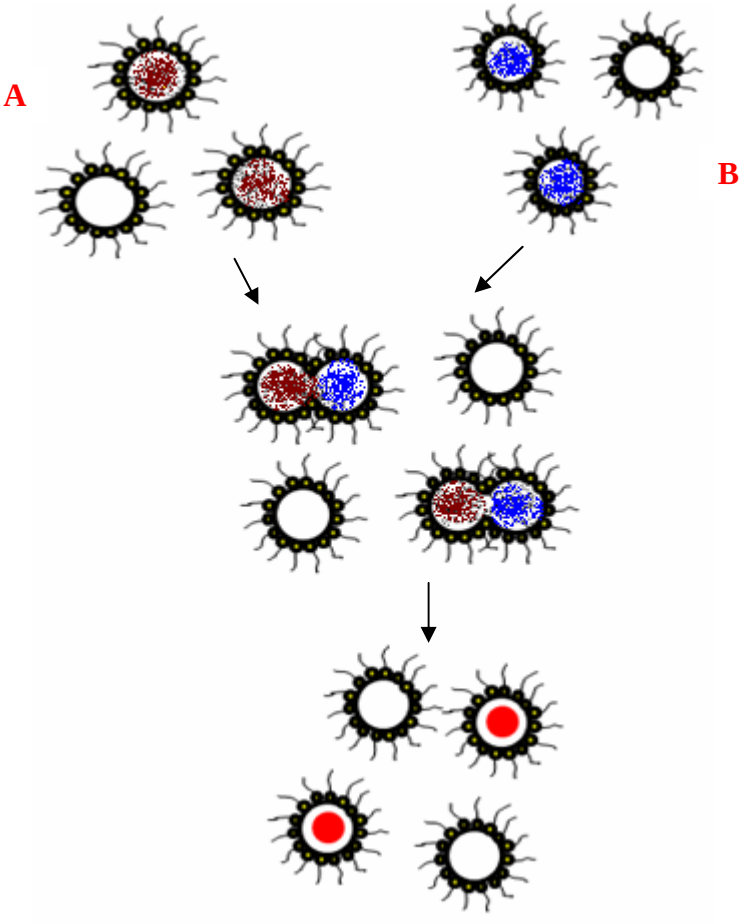

Figure 3.1: Schematic of the nanoparticle formation in microemulsions.

In a general synthesis procedure, one microemulsion contains the salt to be reduced in its aqueous core and the other one consists of reducing agent. These two microemulsions are mixed and the micelles, undergoing Brownian motion, collide with each other to form transient short lived dimers in which the contents are exchanged leading to the formation of nuclei atoms that will subsequently grow to nanoparticles. The presence of surfactant provides steric stabilization against particle aggregation [9]. This process has been widely used for synthesizing colloidal metal, bimetallic, semiconductor and various metal oxide nanoparticles.

Noble metals like gold [10] and silver [11], bimetallic nanoparticles like gold-silver [12] and Fe-Pt [13], semiconductors like CdS [14] and ZnS [15] and metal oxides like iron oxide and CeO_2 [16] have been synthesized using microemulsions.

Pileni et al. [17] have synthesized triangular CdS nanocrystals with 10 nm sides in $Cd(AOT)_2$/isooctane/water reverse micelles. These nanocrystals have been synthesized by bubbling H_2S gas through the $Cd(AOT)_2$/isooctane/water microemulsion under vigorous stirring. But a general method for synthesizing shape controlled particles is yet to be found. Though the aqueous core radius of the microemulsion is proportional to water/surfactant ratio, the ultimate particle size depends upon many other parameters like co-surfactant, type of solvent, surfactant-solvent interaction etc [18].

3.6 Conclusions

This chapter gave a brief overview of microemulsions and the parameters that influence the structure of microemulsions such as packing parameter and HLB. Water in oil microemulsions are used for synthesizing various kinds of nanoparticles. In this study, gold nanoparticles were synthesized in water/AOT/Brij 30 (& Brij 52)/isooctane mixed microemulsions. FePt nanoparticles were synthesized using water/Brij 52/isooctane microemulsions.

3.7 References

1. I. Danielsson and B. Lindman, 'The definition of microemulsion', *Colloids and Surfaces*, 3, 1981, 391.
2. J. H. Schulman, W. Stoeckenius, and M. Prince, *Journal of Physical chemistry*, 63, 1959, 1677.
3. D. Langevin, 'Microemulsions-Interfacial Aspects' *Advances in Colloid and Interface Science,* 34, 1991, 583-595.
4. M. P. Pileni, 'Water in oil colloidal droplets used as microreactors', *Advances in Colloid and Interface Science*, 46, 1993, 139-163.

5. I. Capek, 'Preparation of metal nanoparticles in water-in-oil (w/o) microemulsions', A*dvances in Colloid and Interface Science*, 110, 2004, 49-74.
6. V. T. Liveri, 'Controlled synthesis of nanoparticles in microheterogeneous systems' *Springer publications*, 2006.
7. P. D. I. Fletcher, A. M. Howe, and B. H. Robinson, 'The kinetics of solubilisate exchange between water droplets of a water-in-oil microemulsion', *Journal of Chemical Society, Faraday Transactions*, 1, 83, 1987, 985-1006.
8. L. M. M. Nazario, T. A. Hatton and J. P. S. G. Crespo, 'Nonionic co-surfactants in AOT reversed micelles: Effect on percolation, size, and solubilization site', *Langmuir*, 12, 1996, 6326-6335.
9. Luic M. Liz-Marzan, 'Nanoscale Materials', Kluwer academic publishers 2004.
10. C. L. Chiang, 'Controlled growth of gold nanoparticles in AOT/$C_{12}E_4$/Isooctane mixed reverse micelles', *Journal of Colloid and Interface Science, 239,* 2001, 334–341.
11. W. Zhang, X. Qiao, and J. Chen, 'Synthesis of nanosilver colloidal particles in water/oil microemulsion', *Colloids and Surface A: Physicochemical Engineering Aspects* 299, 2007, 22-28.
12. A. Pal, S. Shah, and S. Devi, 'Preparation of silver, gold and silver-gold bimetallic nanoparticles in w/o microemulsion containing TritonX-100' *Colloids and Surfaces A: Physicochemical Engineering Aspects* 302, 2007, 483-487.
13. Q. Yan, A. Purkayastha, T. Kim, R. Kroger, A. Bose, and G. Ramanath, 'Synthesis and Assembly of Monodisperse High-Coercivity Silica-Capped FePt Nanomagnets of Tunable Size, Composition, and Thermal Stability from Microemulsions' *Advanced Materials,* 18, 2006, 2569-2573.
14. Y. Li, V. P. Kotzeva, and D. J. Fray, 'Electrical performance of CdS nanomaterials synthesized by microemulsion techniques', *Materials letters,* 60, 2006, 2743-2746.

15. H. Tang, G. Xu, L. Weng, L. Pan, and L. Wang, 'Luminescence and photophysical properties of colloidal ZnS nanoparticles', *Acta Materialia*, 52, 2004, 1489-1494.
16. A. Bumajdad, J. Eastoe, M. I. Zaki. R. K. Heenan, and L. Pasupulety, 'Generation of metal oxide nanoparticles in optimized emulsions', *Journal of Colloid and Interface Science,* 312, 2007, 68-75.
17. N. Pinna, K. Weiss, H. Sack-Kongehl, W. Vogel, J. Urban, and M. P. Pileni, 'Triangular CdS Nanocrystals: Synthesis, Characterization and Stability' *Langmuir*, 17, 2001, 7982-7987.
18. C. L. Kitchens, M. C. McLeod, and C. B. Roberts, 'Solvent effects on the growth and steric stabilization of copper metallic nanoparticles in AOT reverse micelle systems', *Journal of Physical Chemistry B*, 107, 2003, 11331-11338.

Chapter 4

Experimental section

Gold nanoparticles were synthesized in water/AOT/Brij30/Isooctane microemulsions. The first part of this chapter describes the experimental protocol and the experimental set-up used to synthesize gold nanoparticles. The second part of this chapter describes the different characterization techniques that have been used to characterize nanoparticles.

4.1 Synthesis of gold nanoparticles in microemulsions

The metal precursor tetrachloroauric acid, surfactant Sodium 2-ethylhexylsulfosuccinate (AOT) and co-surfactant brij-30 were obtained from Sigma-Aldrich chemicals. The solvent, HPLC grade isooctane was obtained from Merck Co. and the reducing agent hydrazine hydrate was obtained from S.D. Fine chem. Ltd. All chemicals were used without any further purification. De-ionized water (Millipore) was used for the work. All glassware was cleaned with freshly prepared aquaregia, rinsed with tap water, de-ionized water and then ethanol before being dried at room temperature.

Water/AOT/Brij30/isooctane mixed microemulsions were prepared following the procedure used by Girish [1]. In repeating some of the experiments with Teflon tube for injecting hydrazine, the concentrations of the reagents used were same as the concentrations used by Girish [1]. Stoichiometrically required hydrazine for reducing gold chloride was calculated based on the following reaction reported in the literature [2].

$$4HAuCl_4 + 3N_2H_5OH \rightarrow 4Au + 16HCl + 3N_2 + 3H_2O \quad \text{..... (2.1)}$$

The concentrations of aqueous gold chloride and hydrazine hydrate solutions were taken appropriately such that the water to surfactant molar ratio (W_0) was maintained at a value of eight in both microemulsions. Gold nanoparticles were synthesized by injecting hydrazine hydrate microemulsion into gold chloride microemulsion at a known rate, which is controlled by a stepper motor. Solutions were mixed using a standard 4-blade Rushton impeller (made of Teflon) in a 100 ml beaker fitted with a four legged baffle [1].

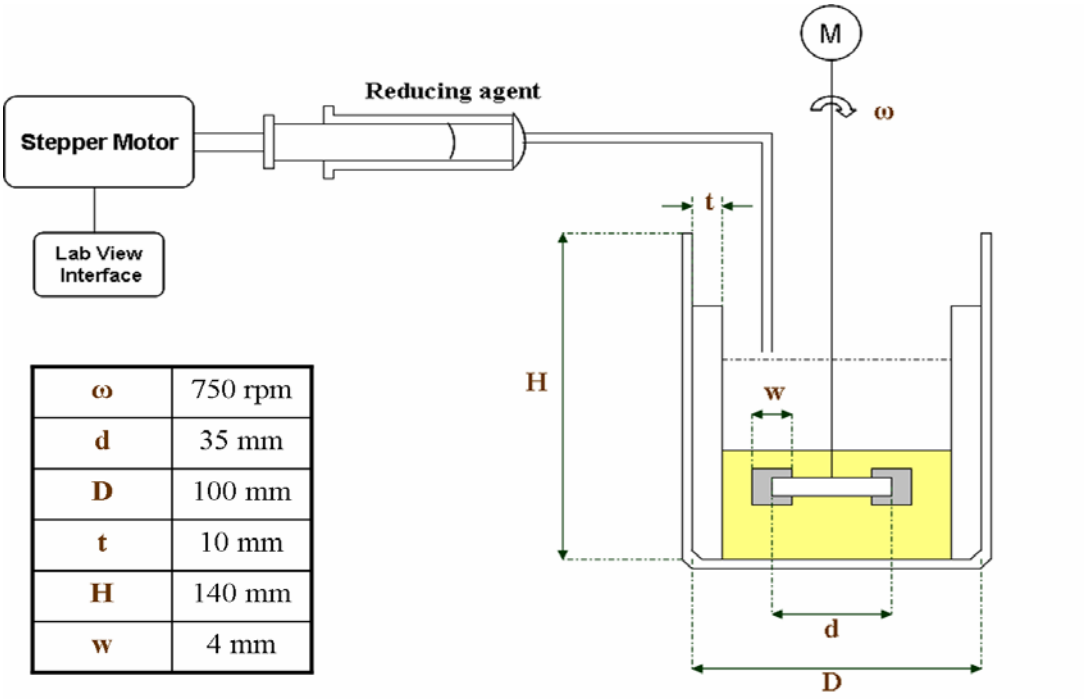

ω	750 rpm
d	35 mm
D	100 mm
t	10 mm
H	140 mm
w	4 mm

Figure 4.1: A schematic of the experimental set-up showing the injection of hydrazine microemulsion into the metal salt precursor solution using a stepper motor.

4.2 Sample characterization

Ultraviolet-Visible spectroscopy, Dynamic Light Scattering (DLS), Transmission Electron Microscopy (TEM) and X-ray diffraction (XRD) were the

characterization tools employed for characterizing the nanoparticles synthesized in microemulsions. Though UV-Visible spectroscopy cannot be used unambiguously to quantify the nanoparticle size, it can be used to detect the presence of nanoparticles because noble metals exhibit a strong absorption band in UV-Visible range. Dynamic light scattering technique characterizes the nanoparticles by means of an effective diffusivity whereas TEM is a direct imaging technique. X-ray diffraction technique is used to determine the crystal structure.

4.2.1 Dynamic Light Scattering (DLS)

Dynamic light scattering is also known as photon correlation spectroscopy or quasi elastic light scattering. This is one of the most popular methods to measure the size of the particles, which are typically in submicron range. The lower size limit of this type of measurement is determined by the detectable scattering fluctuations of particles versus the experimental noise. The upper size limit of these measurements is determined primarily by the sedimentation limit; particles that are being analyzed must be stably suspended.

4.2.1.1 Set-up

DLS comprises of a He-Ne laser source (Model: Melles Griot 75 mW; length: 1m) operated at 633 nm, a BI-200SM goniometer (Brookhaven Instruments Co.) and an avalanche photodiode (APD) detector as shown in Figure 4.2. The laser beam passes through a neutral density filter (with an optical density of 3) and lens assembly, which focuses the laser beam to the sample cell assembly. The sample cell assembly contains a vat, which is filled with index matching liquid, decahydronaphthalene (decalin) used to reduce the scattering from interfaces. The scattered light from sample cell assembly is detected by detector assembly. The front portion of the detector optic assembly consists of an eyepiece which focuses the light

onto an aperture. The pinhole wheel is used to change the aperture size. The filter wheel is used to allow the beam of desired wavelength. The filtered beam then passes to an avalanche photodiode (APD) which detects the temporal fluctuations of the scattered light intensity from the sample. These fluctuations are fed to the correlator.

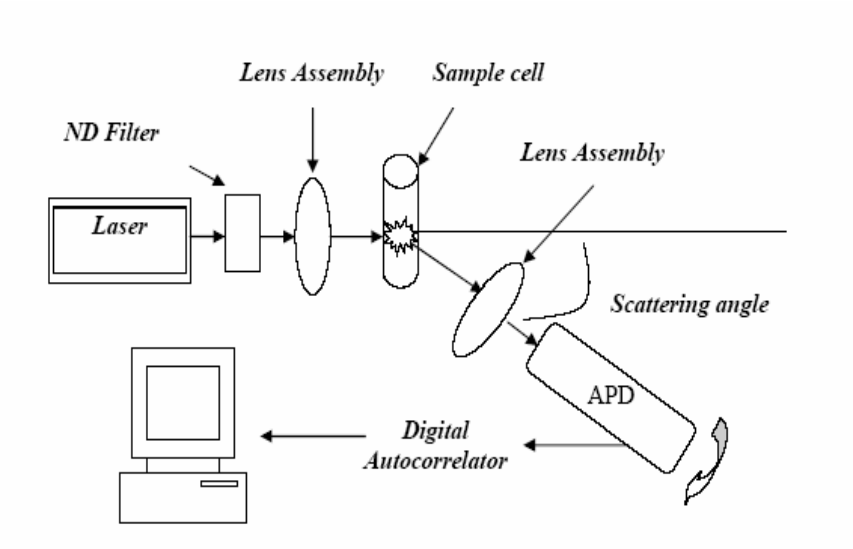

Figure 4.2: Schematic representation of DLS set-up [3]

In this study, the dynamic light scattering instrument (Model BI-200SM) from Brookhaven instruments Co. with BI-9000AT correlator system is used, which has an adjustable delay range capable of producing continuous correlation function starting from 100 ns. For nanoparticle characterization, 200μm or 400μm aperture size and 633 nm filter were be used and the intensity measurements were obtained at a scattering angle of 90^0 in order to minimize the effects of dust and misalignment. The mean particle size and polydispersity can be estimated either by using the method of cumulants or by using packages for inverse Laplace transform like nonnegatively constrained least squares (NNLS) method, CONTIN etc.

4.2.1.2 Principle of operation

In DLS, a monochromatic laser beam such as a laser is focused onto a sample containing particles that are in Brownian motion. Because of this Brownian motion of the particles, the interference pattern formed at the detector and the scattering intensity measured by the detector changes with time. Since the incoming light is a laser, which has high intensity and optical stability, the fluctuations in the intensity of the scattered light can be measured. The translational diffusion coefficient of the particle is measured based on the autocorrelation function, which represents the correlation between the two scattered light signals different in time domain. The fluctuations in the scattered light intensity caused by the Brownian motion of the particles are detected by the APD detector. These fluctuations are correlated using digital autocorrelator to obtain diffusion coefficient (D_t) of the particles from which the hydrodynamic diameter (d_H) is calculated from Stokes-Einstein equation.

$$D_t = \frac{K_B T}{3\pi\eta d_H} \quad \text{……..……..…..…..} (4.1)$$

Where, K_B is the Boltzmann's constant. η is the viscosity of the sample at temperature T.

4.2.1.3 Determination of diffusion coefficient

The second order auto-correlation function (ACF) is given by

$$C(\tau) =< n(\tau)n(t-\tau) > \text{…….……..…..} (4.2)$$

Where, $n(\tau)$ is the number of photons counted over a sampling interval $\Delta\tau$ centered at time t and $n(t-\tau)$ is the number of photons counted over $\Delta\tau$ but delayed in time by τ .

The normalized scattered intensity time autocorrelation function of the scattered light intensity can be written as (called as Siegert relation)

$$C(\tau) = \left(1 + \gamma \left| g^1(\tau) \right|^2 \right) \quad \text{……..……..…..} \quad (4.3)$$

Where, γ is a constant determined by the specific experimental setup and $g^1(\tau)$ is the normalized first order time autocorrelation function.

For a dilute solution of monodisperse nanoparticles, it can be shown that $g^1(\tau)$ is a single exponential whose time decay is determined by the translational self-diffusion coefficient of the particle D and the length of the scattering vector q.

$$g^1(\tau) = \exp(-q^2 D\tau) \quad \text{……..…..…..….} \quad (4.4)$$

The scattering wave vector length depends on the scattering angle θ, and the wavelength λ of the light in the scattering medium:

$$q = (4\pi/\lambda) \sin(\theta/2) \quad \text{……..…….……..…..} \quad (4.5)$$

Nanoparticle dispersions are often polydisperse; i.e. there will be particles with a distribution of sizes. The particles in distribution thus have different translational self-diffusion coefficients. So the particles with a given diffusion coefficient contributes its own exponential to the first order correlation function.

$$g^1(\tau) = \sum A_i \exp(-\Gamma_i \tau)$$

$$\text{……..……..…....…} \quad (4.6)$$

Where, $\Gamma_i = q^2 D_i$ is the reciprocal decay time and A_i is a weighting factor proportional to the fraction of the scattered intensity contributed by this subset of particles.

In the cumulants method, the logarithm of autocorrelation function (ACF) is expanded as a power series over time in which the coefficients are the cumulants. The first cumulant is equal to the average of the reciprocal relaxation time. The second cumulant is a measure of dispersion. “Poly” refers to the ratio of second cumulant to the square of the first cumulant. If the second and higher order cumulants are zero, the ACF is a single exponential. If the sample is polydisperse, there will be a distribution of diffusion coefficients.

Alternatively, an inverse Laplace transform can be performed on the experimental data to obtain the distribution function. Mathematical techniques for performing such transforms are known as regularization techniques. In NNLS, the

criterion used to select the possible solution out of all the solutions fitting the data is that distribution functions are represented by positive numbers. A different version called CONTIN finds the smoothest non-negative correlation function consistent with the data. In addition to positive constraints, CONTIN selects the simplest solution i.e. one which gives least information for the distribution function [4].

4.2.1.4 Sample preparation

For avoiding heterogeneous nucleation during the synthesis and for smooth operation in DLS, samples must be free of dust particles. Since the scattered intensity is proportional to the sixth power of particle diameter [5], the intensity of scattering due to a sub-micron size particle will be negligible when compared with the scattered intensity from a micron size particle. So care has to be taken to avoid scattering due to dust particles in the following steps.

- preparing the sample (Chemicals, glass wares, water used)
- sample cell cleaning
- filtration of index matching liquid

Sample cells were cleaned using 2 % solution of Micron-90 solution (Cole-Parmer) at 60^0 C, de-ionized water and ethanol. The index matching liquid, Decalin can be filtered with the help of an externally connected filtration system.

4.2.1.5 Factors affecting DLS performance [5]:

Fluctuations in the average count rate (ACR) must be minimized. Intermediate jumps in the ACR indicate the presence of dirt in the sample or in Decalin. ACR should decrease with the dilution of the sample with solvent. Increase of ACR with dilution indicates that the sample is in the multiple scattering regime in which the temporal fluctuations of the scattering intensity are not random. Multiple scattering

can be avoided by diluting the sample with solvent but excess dilution reduces ACR signal. ACR should always be in the recommended range of 10 kilo counts per second (kcps) to 200 kcps**.** This can be obtained by adjusting either ND filter or pinhole wheel or filter wheel. Also, the plot of ACR with time should not have any slope. Slope indicates the presence of interaction between the particles, which leads to aggregation.

One more important parameter to be considered in DLS characterization is baseline difference, which is reported in the correlator control window. Baseline difference refers to the difference between the measured baseline and the calculated baseline. Calculated baseline is obtained from a fit of the data using Siegert relationship, and is compared with the measured baseline of long τ, delay time. The baseline difference must be positive and less than 1%. Negative baseline difference can be avoided by increasing the sample measurement time. High baseline difference indicates the presence of bigger size particles, probably dirt. This can be avoided only by removing dirt from the scattering volume. Hydrodynamic diameter calculated from the Stokes-Einstein equation depends on various parameters like temperature and viscosity of the sample. Hence, these properties can affect the result but their effect is not as significant as the effect of dirt.

Delay time is the other important parameter which can affect the result. There are two delay times namely initial and final. The motions of the particles are correlated when the time scale of detection is small. Smaller particles diffuse faster when compared with larger size particles. Hence, delay time chosen for the smaller particles should be small when compared with the larger size particles. The initial delay and final delay times has to be chosen in such a way that a smooth exponential decaying ACF is obtained. For sub-micron size particles, initial delay times must be in the range of 2 to 5 μs while final delay time can be in the order of few seconds.

4.2.1.6 Sampling procedure

The samples prepared were characterized with DLS without filtration. Appropriate concentration was used to avoid multiple scattering and inter particle interaction. Non-negatively constrained least squares (NNLS) method was used to get size distribution from the autocorrelation function. The scattered intensity is proportional to the sixth power of the diameter of the particles i.e. the intensity plot is biased towards the larger particles. Since the number plot is biased towards very small particles (of the size of solvent molecules), intensity plot was used to get the mean size and size distribution giving importance to the peak height to select dominant mode in the distribution. A Gaussian curve was fitted to this distribution to get the mean size. DLS reading was measured six times for each sample (as per the recommendation of ISO 13321 for particle size analysis – Photon correlation spectroscopy [6]). Standard error of the mean was reported with 95 % confidence, where limits were calculated using critical values of student's *t* distribution. The size was reported as $\bar{x} \pm$ C where C represents the confidence limits of mean for sample size of 6.

4.2.2 UV-Visible spectroscopy

Optical properties of metal nanoparticles have been fascinating many scientists since 19th century. Colloidal gold is responsible for the red color seen in stained glass windows of 17th century [7]. Mie was the first to explain this phenomenon by solving Maxwell equations that describes the extinction spectra of spherical particles of arbitrary size [8]. When a metal nanoparticle is irradiated by light, the oscillating electric field interacts with conduction electrons due to which the electron cloud gets displaced slightly. When the electron cloud gets displaced relative to the nuclei, a restoring columbic force between oppositely charged electron cloud and nuclei causes the electron cloud to oscillate relative to the nuclei. This collective oscillation of electrons is called the plasmon resonance of the particle [8]. The frequency (or wavelength) at which this occurs can be used to characterize the nanoparticles. For gold and silver this phenomenon occurs in visible light regime.

For characterizing the gold nanoparticles synthesized, UV-Visible spectrophotometer (PG Instruments, T60U Spectrophotometer) was employed. A known sample dilution (1 ml of sample to 2 ml of isooctane) was used and scanned over a wavelength range of 200 to 900 nm with a resolution of 1 nm. For changing the pH of aqueous phase in micelles, 0.1 ml of 1M HCl was added to the diluted sample (1ml of sample + 2 ml of isooctane). Isooctane was used to collect background spectra.

4.2.3 Transmission electron microscopy (TEM)

Transmission Electron Microscopy (TEM) is an imaging technique, in which electrons are used to image particles. In ordinary light microscopes, the minimum particle size that can be imaged is limited by the wavelength of the light. However, the use of electrons in TEM has made possible image resolution of the order of Angstroms. In TEM, electromagnetic lenses are used to focus the electrons into a collimated beam. Some electrons are transmitted through sample depending on the specimen under analysis. The transmitted electrons are used to form the image. TEM analysis (using Tecnai G30, Nanoscience initiative center, Indian Institute of Science) was performed on one sample and results are presented in chapter 5. TEM sample was prepared by placing 50 drops of the solution on a carbon grid, which is placed on a tissue paper. It was dipped in acetone to remove excessive surfactant and dried by blowing nitrogen gas across the grid.

4.2.4 X-ray diffraction (XRD)

In this technique, x-rays are used to determine the crystal structure of the sample. Diffraction occurs when the radiation interacts with a periodic structure whose periodic distance is similar to the wavelength of the radiation. Wavelengths of x-rays are in the order of angstroms, which is in the range of typical interatomic

distances in crystalline materials. Hence the x-rays diffracted from crystalline materials contain information about the structure of the unit cell. Each crystalline material has its unique characteristic diffraction pattern, which can be used for its identification [9]. The x-rays most commonly used are emitted by copper whose characteristic wavelength of K radiation is 1.5418 A^o. When the incident beam strikes the sample, diffraction occur at all possible orientations (2θ) and the diffracted beams are detected by a movable detector. In general, detector scans over a range of 2θ values.

The FePt nanoparticle powder is prepared by precipitating the nanoparticles synthesized in microemulsions by adding ethanol and centrifuging for 20 min at 3000 rpm. The precipitated nanoparticles are washed with acetone to remove the surfactant and vacuum dried to obtain the nanoparticles in powder form. X-ray diffractogram was recorded on JEOL x-ray diffractometer (JDX-8030) with a scan rate of 1^0 2θ min^{-1} over 2θ values ranging from 15^0 to 125^0.

4.3 Conclusions

The main aim of this chapter was to explain the different characterization techniques used for characterizing the nanoparticles synthesized. TEM is a direct imaging technique whereas DLS and UV-Visible spectroscopy confirms the presence of nanoparticles by making use of their properties such as self-diffusion (DLS) and surface plasmon resonance. Also detailed information about the principle involved in DLS and its operating procedure along with the parameters which affect its performance were presented.

4.4 References

1. M. Girish, 'Nanoparticle synthesis in microemulsions', Master of Engineering Report, *Indian Institute of Science,* 2007.

2. C. L. Chiang, ‘Controlled growth of gold nanoparticles in AOT/$C_{12}E_4$/Isooctane mixed reverse micelles’, *Journal of Colloid and Interface Science,* 239, 2001, 334–341.
3. S. P. R. Daliparthi, ‘Synthesis and characterization of gold nanoparticles’, Master of Engineering report, *Indian Institute of Science,* 2006.
4. R. Finsy, ‘Particle sizing by quasi-elastic light scattering’, *Advances in Colloid and Interface Science*, 52, 1994, 79-143.
5. Instruction manual for BI-200SM Goniometer Version 2.0, Third print, Brookhaven Instruments Corporation (BIC), 1993.
6. International standard, ‘ISO 13321: Particle size analysis-Photon correlation spectroscopy’, First edition, 1996-07-01.
7. S. Link and M. A. El-Sayed, ‘Spectral properties and relaxation dynamics of surface plasmon electronic oscillations in gold and silver nanodots and nanorods’, *Journal of Physical Chemistry B*, 103, 1999, 8410-8426.
8. K. L. Kelly, E. Coronado, L. L. Zhao, and G. C. Schatz, ‘The optical properties of metal nanoparticles: the influence of size, shape and dielectric environment’, *Journal of Physical Chemistry B*, 107, 2003, 668-677.
9. http://materials.binghamton.edu/labs/xray/xray.html accessed on 25/06/06.

Chapter 5

Synthesis of gold nanoparticles

5.1 Experiments to understand the presence of unreacted gold chloride

It was suspected that the tube (PVC) used previously may not have been compatible with hydrazine hydrate. Hence it was decided to use a Teflon tube, which is compatible with almost all chemicals for injecting hydrazine microemulsion. Initial experiments were carried to check for the presence of unreacted gold chloride by UV-Visible absorption spectrum and also to measure the size of the particles synthesized. For this experiment, the concentrations of the chemicals used were same as the concentrations used previously [1].

Four different addition rates (addition rates are 1.2 ml/s, 0.6 ml/s, 0.45 ml/s and 0.3 ml/s) were used to synthesize nanoparticles using Teflon tube and 0.45 ml/s injection was repeated with previously used tube for verification. Figure 5.1 shows the UV-Visible absorption spectra of the samples. It is clear from the spectra that the samples synthesized using Teflon tube didn't show any peak other than the gold nanoparticle peak whereas the sample synthesized using PVC tube had a peak at 274 nm indicating the presence of unreacted gold chloride. DLS measurements of the samples are shown in table 5.1.

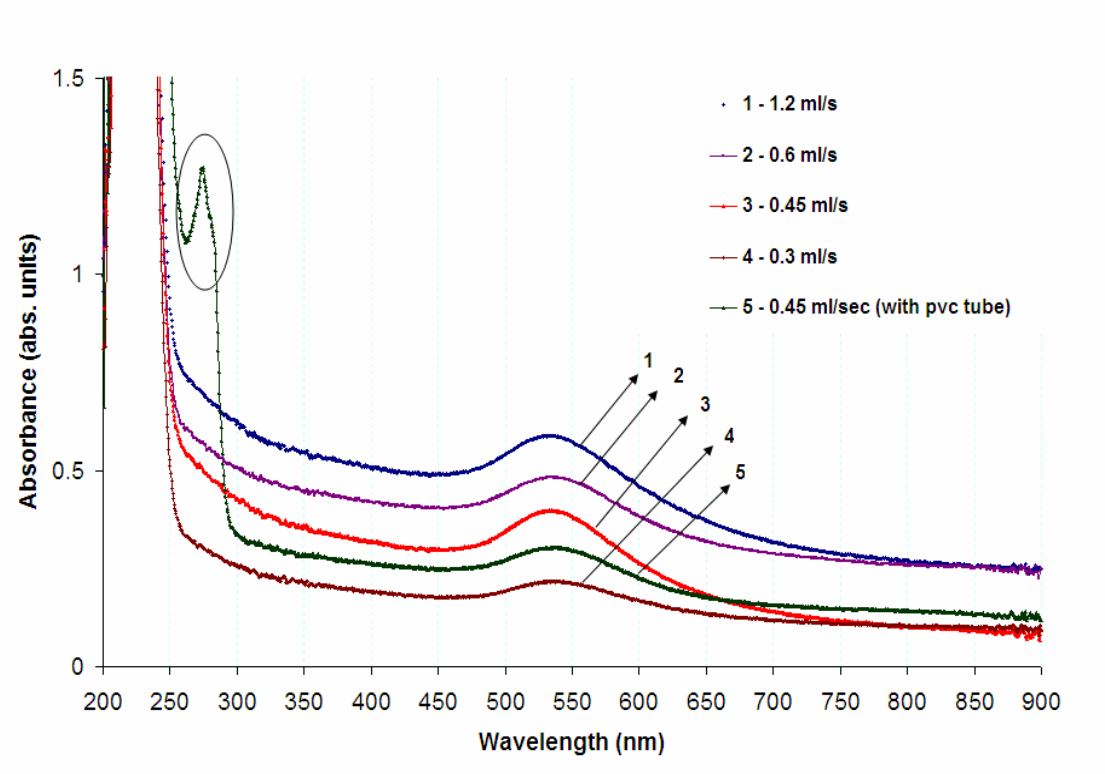

Figure 5.1: UV-Visible spectra of gold nanoparticle solutions synthesized at different addition rates of reducing agent using the modified setup consists of a Teflon tube for injection. Synthesis conditions: [$HAuCl_4$]: 0.03 M; [N_2H_5OH]: 0.3 M; [AOT]: 0.2 M; [$C_{12}E_4$]: 0.2 M; [water]/ [AOT]: 8. Spectra were shifted for clarity.

.

Only 1.2 ml/s and 0.45 ml/s injection rates showed small particles in DLS whereas the other samples showed bigger particles of size greater than 150 nm. Particles synthesized using reducing agent addition rate of 0.6 ml/s and 0.3 ml/s aggregated before characterization. Though the reason was not clear, this experiment showed that PVC was reacting with hydrazine. So it was decided that all future experiments will be done using a Teflon tube.

S. No	Addition rate (ml/s)	Mean size of the particles (nm)	Confidence Limits of the Mean (n = 6 with 95 % confidence)
1	1.20	8	1
2	0.45	8.2	0.4

Table 5.1: Effect of addition rate of hydrazine on particle size. Synthesis conditions: [$HAuCl_4$]: 0.03 M; [N_2H_5OH]: 0.3 M; [AOT]: 0.2 M; [$C_{12}E_4$]: 0.2 M; [water]/ [AOT]: 8.

5.2 Effect of excess hydrazine on stability of nanoparticles

Since the peak for unreacted gold chloride was not observed in the experiment carried on with the Teflon tube, the following experiments were done to study the effect of excess hydrazine on the size and stability of nanoparticles synthesized. The reaction was assumed to be [2]:

$$4HAuCl_4 + 3N_2H_5OH \rightarrow 4Au + 16HCl + 3N_2 + 3H_2O \text{ ……....…} \quad (5.1)$$

Initial experiment was carried on using stoichiometrically required amount of hydrazine hydrate (0.0374M) to reduce gold chloride (0.05M). The color of the gold chloride microemulsion changed from pale yellow to pale pink, dark blue and finally to black color indicating rapid aggregation of the particles even while stirring. The UV-Visible absorption spectra didn't show unreacted gold chloride peak. Then the amount of hydrazine was increased to 3 times the stoichiometrically required amount (molar ratio of hydrazine to gold chloride of 2.25). This time also the particles agglomerated though the pink color (indicating nanoscale gold particles) was stable for longer time. The first three samples prepared using different addition rates yielded agglomerated particles. So for fourth sample hydrazine was added instantaneously (~2 sec) with out stirring. This yielded stable nanoparticle dispersion.

DLS measurement of this sample gave the particle mean as 15 ± 1 nm. The UV-Visible spectra of the sample prepared with three times excess hydrazine (instantaneous addition) and stoichiometrically required hydrazine are shown in Figure 5.2.

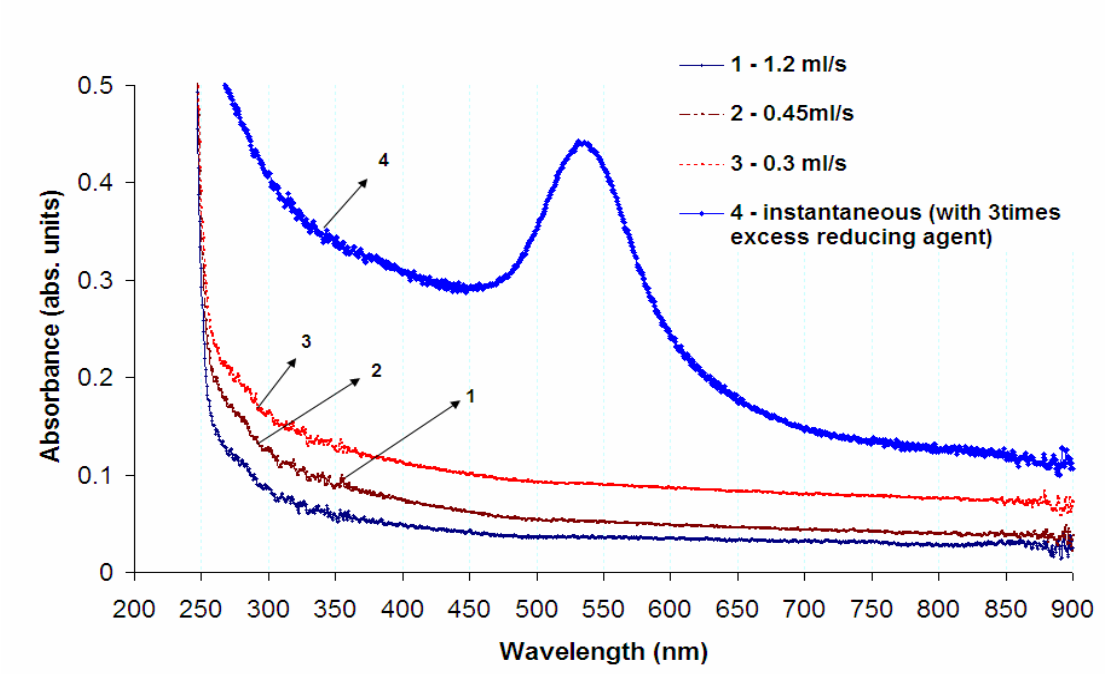

Figure 5.2: UV-Visible spectra of gold nanoparticle solutions synthesized at different addition rates of reducing agent with modified setup. Synthesis conditions: [$HAuCl_4$]: 0.05 M; [N_2H_5OH]: 0.0374 M (for curves 1, 2 and 3) & 0.112 M for 4th curve; [AOT]: 0.2 M; [$C_{12}E_4$]: 0.2 M; [water]/ [AOT]: 8.

Concentration of hydrazine was increased to 0.23 M, which is 6 times excess (molar ratio of 4.5) to that of stoichiometrically required amount. In this case also, only instantaneously added hydrazine gave stable particles whereas the slower addition rates yielded agglomerated particles. One observation is that the pink color of the solution evolved is stable for a longer time as compared to the previous two experiments. DLS measurement of the stable dispersion gave the mean size of the particles as 9.6 ± 1.3 nm. One more experiment was done using 9 times excess hydrazine (molar ratio of 6.75) to study the stability aspect of nanoparticles. The as formed particles were stable for longer time even for slower addition rates and DLS

measurements are shown in Table 5.2. From this study, it was clear that excess hydrazine is somehow making the particles stable for a longer time. By using excess hydrazine even lower addition rates yield stable particles.

S. No	Addition rate (ml/s)	Mean size of the particles (nm)	Confident Limits of the mean (n = 6 with 95 % confidence)
1	1.20	8.9	0.3
2	0.60	11.1	0.4

Table 5.2: Effect of addition rate of hydrazine on particle size. Synthesis conditions: [$HAuCl_4$]: 0.05 M; [N_2H_5OH]: 0.224 M; [AOT]: 0.2 M; [$C_{12}E_4$]: 0.2 M; [water]/ [AOT]: 8.

5.3 Effect of pH on stability of nanoparticles

As excess hydrazine was making the particles more stable, it was decided to study the effect of pH on the stability of gold nanoparticles synthesized in microemulsions. This is because hydrazine hydrate is a strong base apart from being a strong reducing agent [3]. It was reported that hydrazine hydrate can exist as two dissociated forms ($N_2H_5^+$ and $N_2H_6^{2+}$) in aqueous solution [4]. To estimate the pH of the resultant mixture of gold chloride and hydrazine, 2 ml of aqueous gold chloride solution (0.05M) and 2 ml of hydrazine hydrate solution were added separately in a beaker and pH was measured using pH meter (ORION 5 STAR) and is reported in table 5.3. As the pH of the resulting mixture increased (i.e. more basic), the particles synthesized were stable for a longer time. So it was suspected that the stability was not only due to the surfactant but also due to the adsorbed ions on the particle surface.

S. No	Hydrazine concentration (M)	Molar ratio of hydrazine to gold chloride & (pH)	Gold chloride concentration (M)	pH	pH of the mixture in aqueous phase (2 ml gold chloride + 2 ml of hydrazine hydrate)
1	0.0375	0.75 (9.6)	0.05	1.5	1.7
2	0.1125	2.25 (9.8)	0.05	1.5	1.9
3	0.23	4.5 (9.9)	0.05	1.5	2.5
4	0.34	6.75 (10.1)	0.05	1.5	7.2
5	0.50	10.0 (10.2)	0.05	1.5	8.4

Table 5.3: Table showing the pH of hydrazine & mixture of hydrazine and gold chloride at various concentrations of hydrazine hydrate.

Spirin et al have studied the stability of gold nanoparticles in AOT and Triton X-100 microemulsions [5]. They concluded that in the presence of dissolved oxygen, the surface of gold nanoparticles is oxidized to $Au(OH)_4^-$ ions instead of gold oxides. This $Au(OH)_4^-$ forms $Au(OH)_3$ at lower pH according to the following reaction.

$$Au(OH)_4^- \Leftrightarrow OH^- + Au(OH)_3 \quad \text{…….....….. (5.2)}$$

It was concluded that a decrease in pH tends to form $Au(OH)_3$, which rapidly form aggregates and this formation of aggregates makes the nanoparticle dispersion unstable. They were able to synthesize more stable particles by partly preventing the

gold nanoparticle surface from oxidation by i) adding thioglycerol after the synthesis and ii) bubbling the microemulsions with Argon for 5 minutes to remove dissolved oxygen.

After knowing that pH plays an important role in stabilizing the particles even in microemulsions, it was decided to study the effect of pH on the stability of particles. For this study, first the pH of gold chloride was adjusted to a value of 10.5 by adding required amount of potassium carbonate. Only stoichiometrically required amount of hydrazine was used for reducing the gold chloride. Since no color change was observed within the regular stirring time of 25 minutes, stirring was extended to two and half hours. But no stable particles were produced and stirring was stopped after observing the formation of black powder at the bottom of the beaker indicating nanoparticle aggregates.

Experiments at three different addition rates (1.2 ml/s, 3 ml/s, and 4.5 ml/sec) were performed by using gold chloride at pH 8 and stoichiometrically required amount of hydrazine. The first sample (1.2 ml/s) was pale pink after synthesis, while the other samples (3 ml/s and 4.5 ml/sec) were blue in color as shown in Figure 5.3. The UV-Visible absorption spectra are shown in Figure 5.4. DLS shows the presence of bigger particles or flocculates of size range 75-100 nm and intermittently a smaller distribution in the range of 10-25 nm. UV-Visible spectra showed that the absorption peaks were around 550 nm indicating the presence of bigger aggregates in the solution. In fact the blue color of the gold colloid itself indicates the bigger aggregates. But these blue aggregates were stable only for a day. The conclusion we can draw from this experiment is that by changing the pH of gold chloride, the aggregation of the nanoparticles was slowed down because in the previous experiment where the pH of gold chloride was not altered, particles aggregated as soon as they were formed.

1.2 ml/s **3 ml/s** **4.5 ml/s**

Figure 5.3: A digital picture of gold nanoparticles synthesized at different addition rates of reducing agent using modified setup consists of a Teflon tube for injection. Synthesis conditions: [$HAuCl_4$]: 0.05 M; [N_2H_5OH]: 0.0374 M; [AOT]: 0.2 M; [$C_{12}E_4$]: 0.2 M; pH of gold chloride solution: 8; [water]/ [AOT]: 8.

TEM images of the samples were taken and the image of the sample (addition rate of 1.2 ml/s) is shown in Figure 5.5. These TEM images have shown aggregates of small particles with the average size of primary particles varying from 8 to 10 nm. From the above images, it is clear that even though there are small particles of size 8-10 nm, they were not stable enough as individual units. These particles were moving as clusters in the solution, which was observed in DLS as an increased hydrodynamic radius (~80 nm) and by UV-Visible absorption spectra.

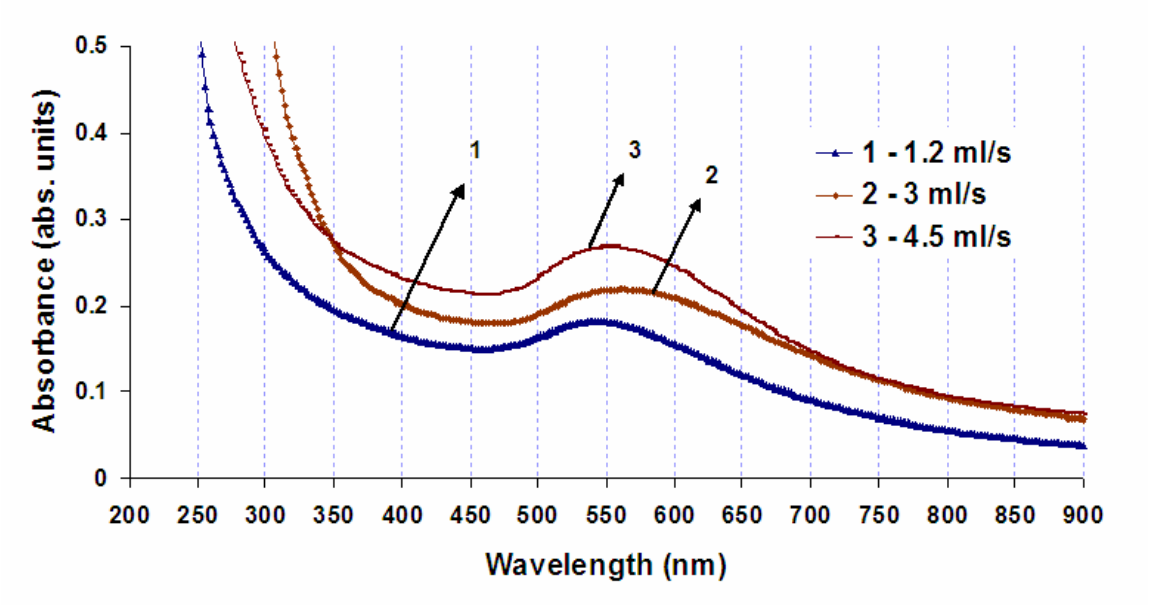

Figure 5.4: UV-Visible spectra of gold nanoparticle solutions synthesized at different addition rates of reducing agent using modified setup consists of a Teflon tube for injection. Synthesis conditions: [$HAuCl_4$]: 0.05 M; [N_2H_5OH]: 0.0374 M; [AOT]: 0.2 M; [$C_{12}E_4$]: 0.2 M; pH of gold chloride solution: 8, [water]/ [AOT]: 8

Since the reaction produces hydrochloric acid, it was assumed that the pH of the solution will be changing with time till the completion of addition of reducing agent. So to avoid rapid changes in pH, it was decided that we should add gold chloride microemulsion to the hydrazine microemulsion, where in the hydrazine will also help in neutralizing the acid produced. It was hypothesized that the hydrochloric acid released in the reaction will be neutralized by the hydrazine present in the solution, there by maintaining the pH at around 8-9. In this experiment, only stoichiometrically required amount of hydrazine was added.

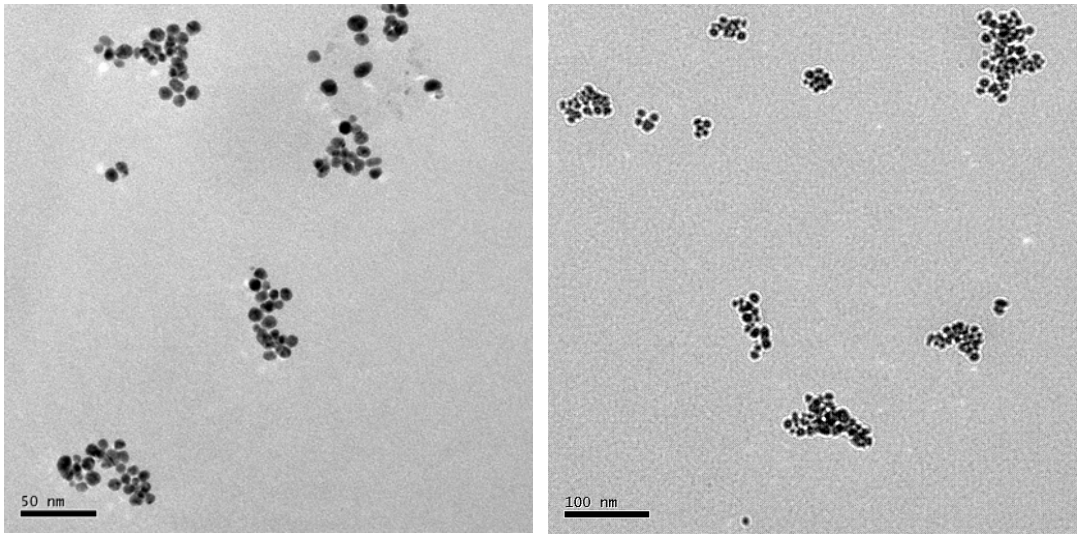

Figure 5.5: TEM image showing clusters of particles at two different magnifications.

This experiment produced gold nanoparticles, which are in reddish pink color, which is a characteristic color of small gold nanoparticles (3-50nm). But the DLS measurement showed the presence of bigger particles or flocculates, which are 100-150 nm in size in all readings. From each sample, half of the solution was taken and kept in the refrigerator to know the effect of temperature on the stability of the particles synthesized. The color of the samples kept at room temperature changed gradually from pink to blue with time. UV-Visible spectra of the samples kept at room temperature were measured and it is shown in Figure 5.6.

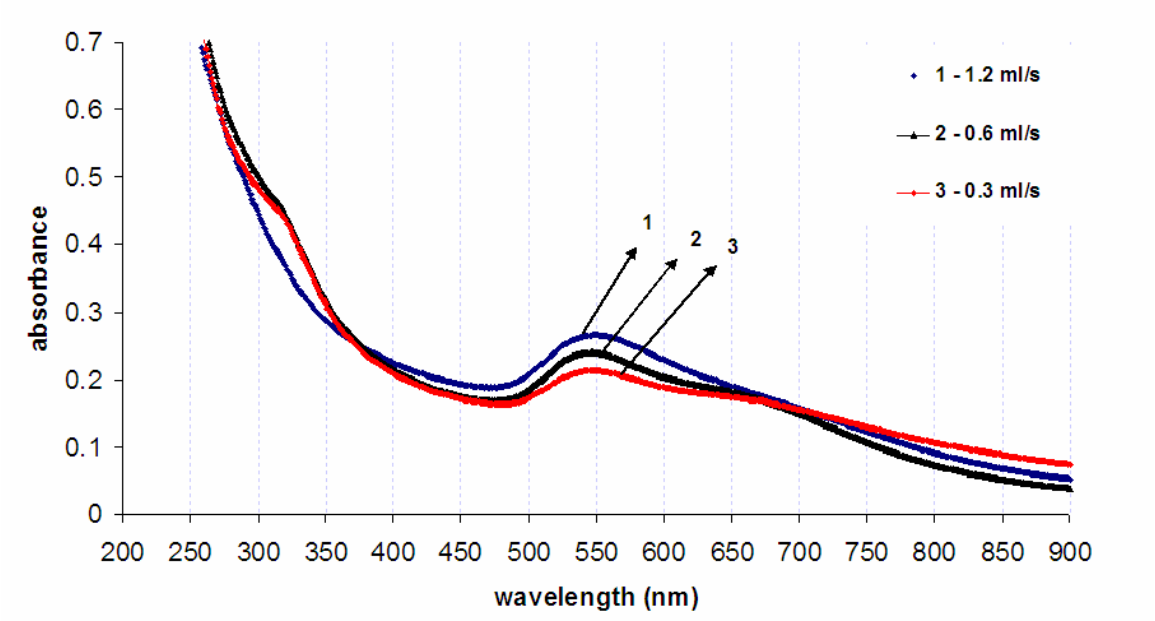

Figure 5.6: UV-Visible spectra of gold nanoparticles synthesized at different addition rates of gold chloride microemulsion using modified setup consisting of a Teflon tube for injection. Synthesis conditions: [$HAuCl_4$]: 0.05 M; [N_2H_5OH]: 0.0374 M; [AOT]: 0.2 M; [$C_{12}E_4$]: 0.2 M; pH of gold chloride solution: 8 and [water]/ [AOT]: 8

From the above spectra, it was observed that the absorption peak was around 550 nm and the shoulder at around 670 nm indicates the presence of non-spherical clusters/aggregates in the solution. Since there was a small shoulder at 312 nm, fixed amount (0.1 ml) of 1M hydrochloric acid was added to change the pH of the solution inside micelles because gold chloride has strong absorbance at lower pH. The UV-Visible spectra of these samples are shown in Figure 5.7.

The spectra showed that there was unreacted gold chloride left in the solution. It was assumed that since hydrochloric acid produced in the reaction was neutralized by the hydrazine, the hydrazine will be consumed even before the gold chloride microemulsion was added completely and hence the appearance of the peak for unreacted gold chloride.

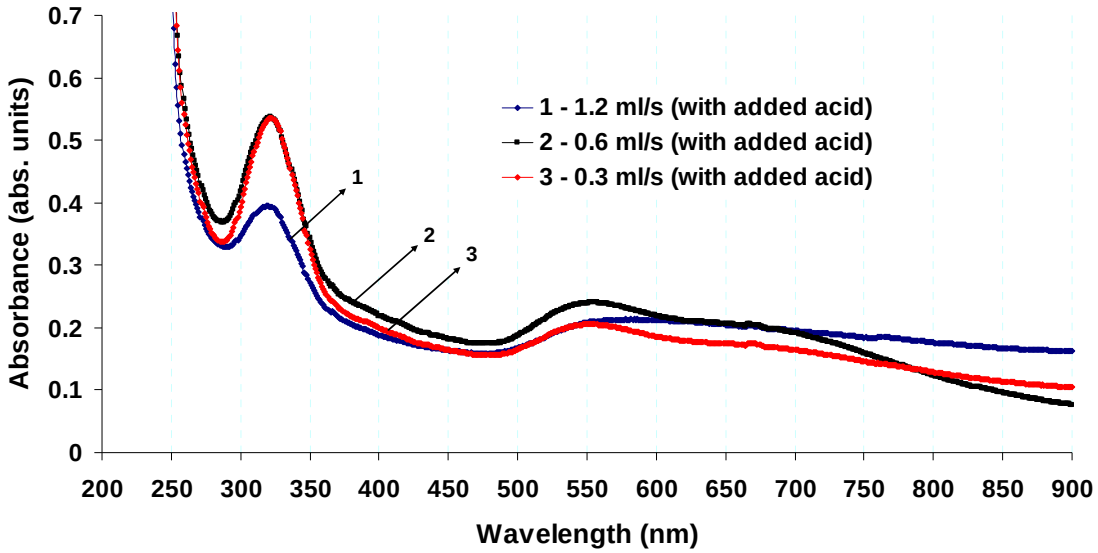

Figure 5.7: UV-Visible spectra of gold nanoparticles synthesized at different addition rates of gold chloride microemulsion using modified setup consisting of a Teflon tube for injection. HCl was added to change the pH inside micelles. Synthesis conditions: [$HAuCl_4$]: 0.05 M; [N_2H_5OH]: 0.0374 M; [AOT]: 0.2 M; [$C_{12}E_4$]: 0.2 M; pH of gold chloride solution: 8 and [water]/ [AOT]: 8

To ascertain the amount of hydrazine needed to completely reduce the gold chloride, the concentration of hydrazine was increased to two times excess and three times excess to that of stoichiometrically required amount. The UV-Visible absorption spectra showed the presence of unreacted gold chloride in the samples prepared using two times excess hydrazine whereas the samples prepared using three times excess hydrazine did not show unreacted gold chloride peak. From these plots it was concluded that three times excess hydrazine is required to completely reduce the gold chloride present. Dynamic light scattering studies showed the presence of a bimodal distribution. Table 5.4 gives the mean sizes at which the modes appear for the samples prepared using three times excess hydrazine.

No clear trend can be observed in mean particle size with addition rate. This can be attributed to the fact that the reactivity of gold chloride decreases with

increasing pH [6]. The presence of two distributions indicates fact that the particles formed aggregating slowly.

S. No	Addition time (sec)	Addition rate (ml/s)	Mean size of 1st peak (nm)	Mean size of 2nd peak (nm)
1	Instantaneous (3-5 sec)	--	4.9	38.1
2	15	1.2	9.4	43.0
3	30	0.6	11.9	46.5
4	60	0.3	5.5	36.2
5	150	0.12	--	41.1
6	300	0.06	--	36.3

Table 5.4: Effect of addition rate of hydrazine on particle size. Synthesis conditions: [$HAuCl_4$]: 0.05 M; [N_2H_5OH]: 0.1125 M; [AOT]: 0.2 M; [$C_{12}E_4$]: 0.2 M; [water]/ [AOT]: 8; pH of gold chloride: 8.

The solutions that were stored at room temperature (23^0 C) agglomerated within 24 hours while the solutions kept in the refrigerator were stable for more than three days. Lowering the temperature will decrease the thermal energy of the particles undergoing Brownian motion and hence the samples will be kinetically stable for a longer time. One more aspect is that the stability of the particles synthesized will be more temperature sensitive because of the higher concentration ([Brij-30] / [AOT] = 1) of co-surfactant brij-30, which is a non-ionic surfactant.

Bulavchenko et al. studied stability of gold nanoparticles synthesized by reducing gold chloride using hydrazine hydrate in Triton N-42 reverse micelles [7]. They concluded that stable gold nanoparticles were formed only at low solubilization capacities (i.e. low ω_0 values) and high hydrazine concentrations. They concluded that hydrazine hydrochloride formed in acidic medium gets chemisorbed on the surface of gold nanoparticles and there by influences their stability.

The gold nanoparticle sample synthesized using a molar ratio of 10 is phase inverted to check for the charge stabilization. Approximately 60 ml of de-ionized water was added instantaneously to 10-15 ml of gold nanoparticle sample under vigorous stirring. This resulted in a turbid dispersion of pink color. This sample is centrifuged for 30 min at 3000 rpm. A slightly turbid pink color solution is present at the bottom of the centrifuge tube with white colored foam at the top, which is the excess surfactant. 10 ml of the slightly turbid solution was taken and 0.25 g of NaCl was added and kept it for 2 hours to check whether the particles are stabilized by adsorbed ions. It resulted in separation of phases with a clear colorless solution at the bottom and slightly pink colored foam at the top. This shows that the particles are covered by surfactant molecules even after the phase inversion.

It was decided to use higher hydrazine concentration (molar ratio of 10) for synthesizing stable nanoparticles even at slower addition rates in order to study the effect of addition rate on mean size of the particles. Further experiments to study the effect of addition rate on mean particle size were performed using hydrazine concentration of 0.5 M (molar ration of 10).

5.4 Effect of addition rate on mean particle size

Since stable particles can be synthesized even for slower addition rates using higher concentrations of hydrazine, hydrazine to gold chloride molar ratio of 10 is used for synthesizing gold nanoparticles. Effect of addition rate was studied for two systems containing two different co-surfactants, Brij 52 and Brij 30. The results obtained using AOT/Brij 52 system for two runs are shown in table 5.5.

The mean particle size obtained for two runs was plotted against addition rate as shown in Figure 5.8. No clear trend was observed in particle size with addition rate for AOT/Brij 52 system.

S. No	Addition rate (ml/s)	Mean size ± C.I (nm) Trial 1	Mean size ± C.I (nm) Trial 2
1	1.2	17.7 ± 1.1	14.3 ± 1.3
2	0.6	11.7 ± 0.4	14.9 ± 0.9
3	0.45	8.0 ± 0.2	15.4 ± 0.5
4	0.3	17.1 ± 1.0	13.5 ± 0.3
5	0.2	14.4 ± 0.5	12.9 ± 0.0

Table 5.5: Effect of addition rate on mean size of gold nanoparticles. Synthesis conditions: [$HAuCl_4$]: 0.05 M; [N_2H_5OH]: 0.5 M; [AOT]: 0.2 M; [Brij 52]: 0.1 M; [water]/ [AOT]: 8.

It was reported that the addition of nonionic surfactants with larger head groups (Brij 30 and Brij 56 etc.) to AOT/isooctane system increases the fluidity of the interface and interdroplet interaction where as addition of nonionic surfactants with smaller head groups (Brij 52 and Brij 72) decrease both [8]. This decrease in interdroplet interaction will slow down the material exchange between droplets, which is the rate determining step for instantaneous reactions in microemulsions [9].

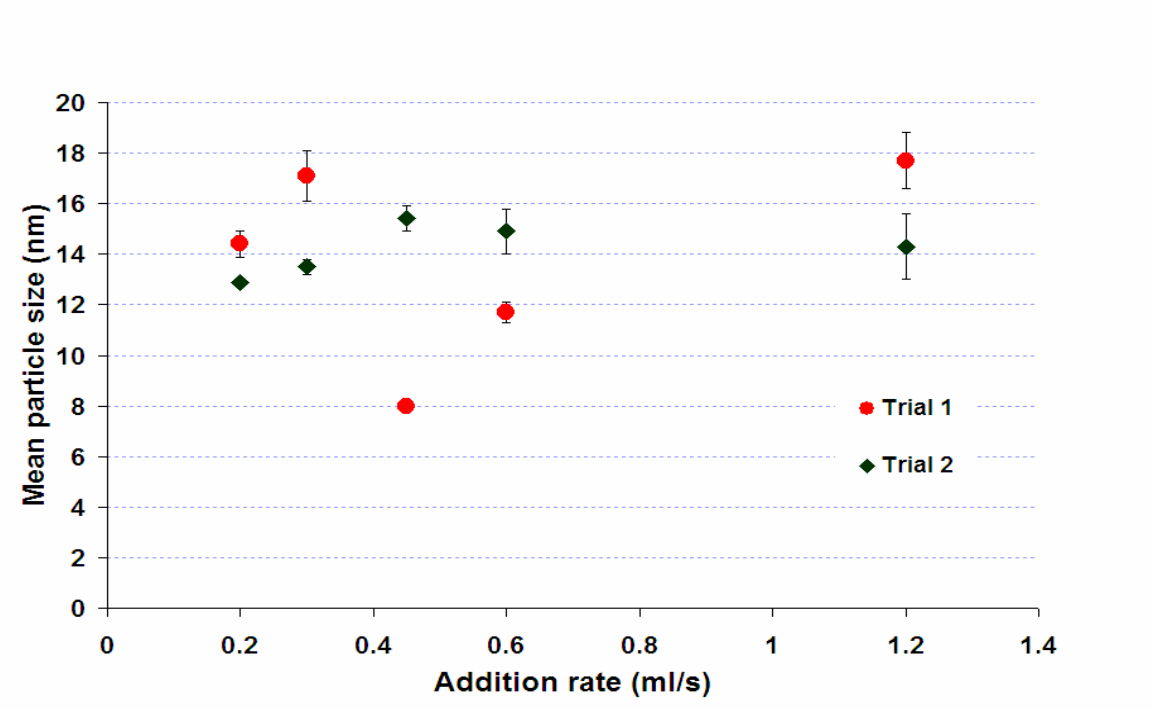

Figure 5.8: Effect of addition rate of hydrazine on mean particle size of gold nanoparticles. Synthesis conditions: [$HAuCl_4$]: 0.05 M; [N_2H_5OH]: 0.5 M; [AOT]: 0.2 M; [Brij 52]: 0.1 M; [water]/ [AOT]: 8.

The effect of addition rate on mean particle size was studied for AOT/Brij 30 system. The main objective of this study is to check the reproducibility of the addition rate study and the trend that was reported [1]. Effect of addition rate was studied at two different temperatures, 25^0C and 30^0C. The results obtained were compared with the data obtained by Girish [1]. Mean particle size obtained using various addition rates at two different temperatures are reported in table 5.6.

S. No	Addition rate (ml/s)	Mean particle size ± C.I (nm) at 25^0C	Mean particle size ± C.I (nm) at 30^0C
1	1.2	11.9 ± 0.5	14.0 ± 0.6
2	0.6	13.1 ± 0.3	14.3 ± 0.6
3	0.45	13.4 ± 0.2	13.7 ± 1.1
4	0.36	13.3 ± 0.2	16.4 ± 0.6
5	0.3	18.2 ± 0.3	14.4 ± 0.9
6	0.24	13.8 ± 1.9	15.8 ± 1.7
7	0.20	15.5 ± 1.3	--

Table 5.6: Effect of addition rate on mean size of gold nanoparticles at two different temperatures, 25^0 C and 30^0 C. Synthesis conditions: [$HAuCl_4$]: 0.05 M; [N_2H_5OH]: 0.5 M; [AOT]: 0.2 M; [Brij 52]: 0.1 M; [water]/[AOT]: 8.

Figure 5.9 and 5.10 show the comparison of the mean particle sizes obtained at 25^0C and 30^0C. These results confirmed the trend of particle size with decrease in addition rate reported by girish [1]. At 25^0 C, mean particle size increased from 11.9 ± 0.6 nm to 15.5 ± 1.8 nm as addition rate decreased from 1.2 ml/s to 0.2 ml/s. At 30^0 C, there is only a marginal increase in size with decrease in addition rate. Mean particle size changed from 14.0 ± 0.8 nm to 16.1 ± 2.2 nm as addition rate decreased from 1.2 ml/s to 0.24 ml/s.

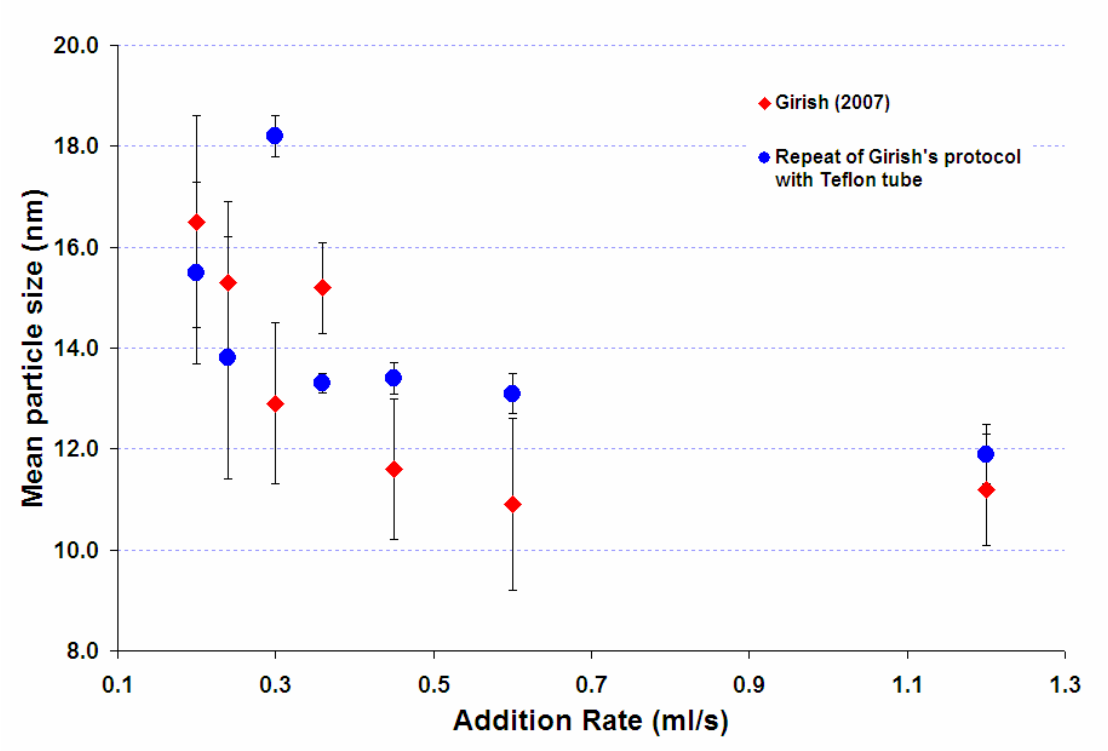

Figure 5.9: Effect of addition rate on mean size of gold nanoparticles at 25^0 C. Synthesis conditions: [$HAuCl_4$]: 0.05 M; [N_2H_5OH]: 0.5 M; [AOT]: 0.2 M; [Brij 52]: 0.1 M; [water]/ [AOT]: 8.

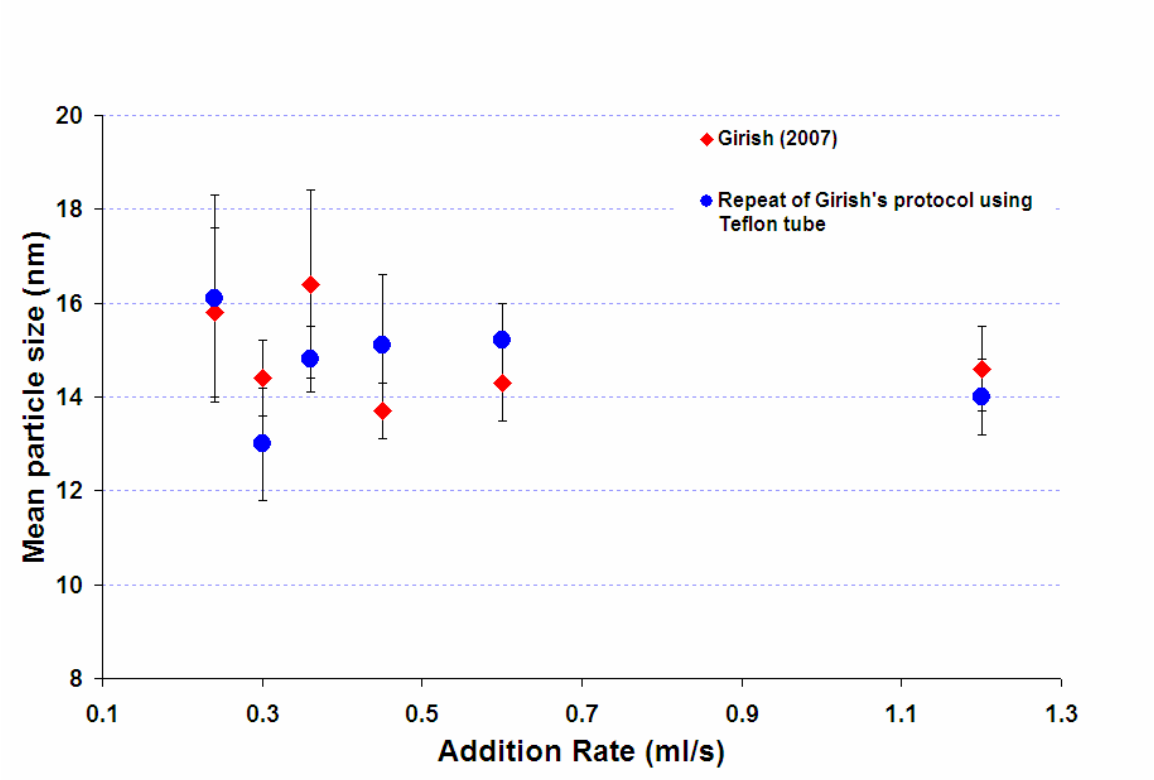

Figure 5.10: Effect of addition rate on mean size of gold nanoparticles at 30^0 C. Synthesis conditions: [$HAuCl_4$]: 0.05 M; [N_2H_5OH]: 0.5 M; [AOT]: 0.2 M; [Brij 52]: 0.1 M; [water]/ [AOT]: 8.

5.5 Color transition time

The pale yellow color of the gold chloride solution changes to colorless, pink and then to deep red indicating the formation of gold nanoparticles. The time taken for the appearance of pink color was measured and compared with the color transition times reported by girish [1]. Figure 5.11 and 5.12 show the comparison of color transition times at 25^0 C and 30^0 C respectively. The color transition times matched well with the previously reported values. The decrease in color transition time with increase in temperature indicates faster exchange of material between droplets.

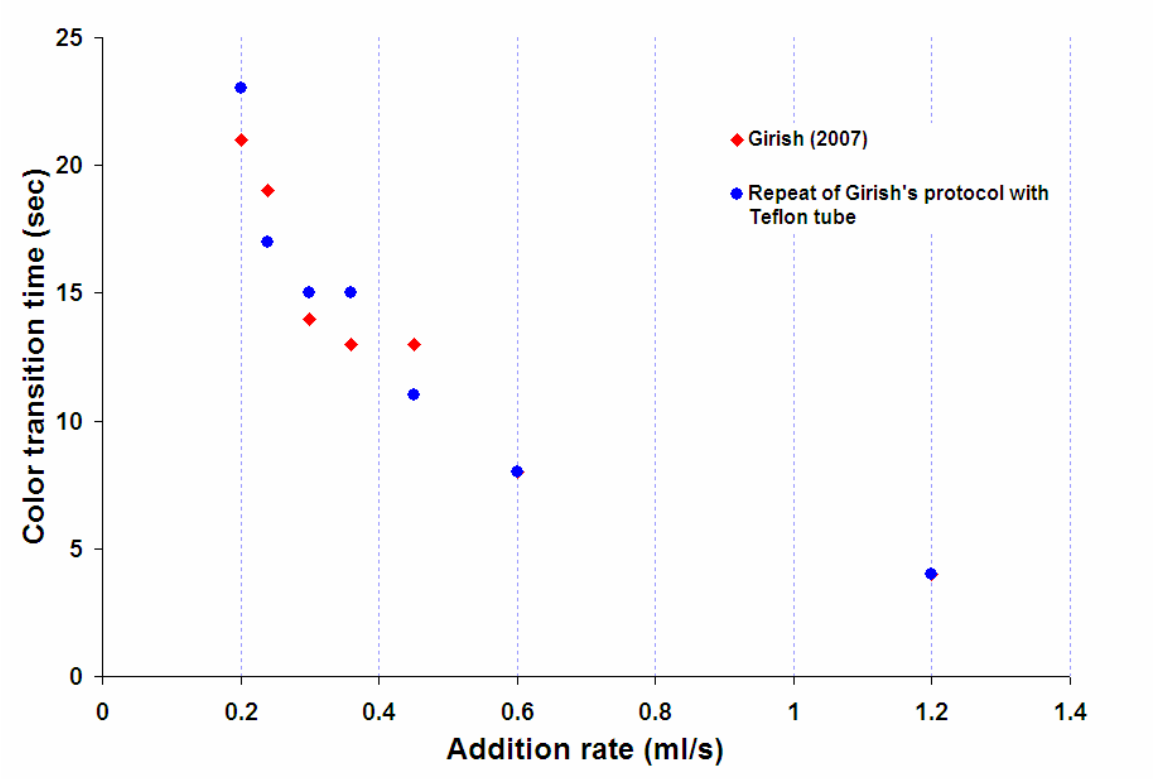

Figure 5.11: Effect of addition rate on color transition time at 25^0 C. Synthesis conditions: [$HAuCl_4$]: 0.05 M; [N_2H_5OH]: 0.5 M; [AOT]: 0.2 M; [Brij 52]: 0.1 M; [water]/ [AOT]: 8.

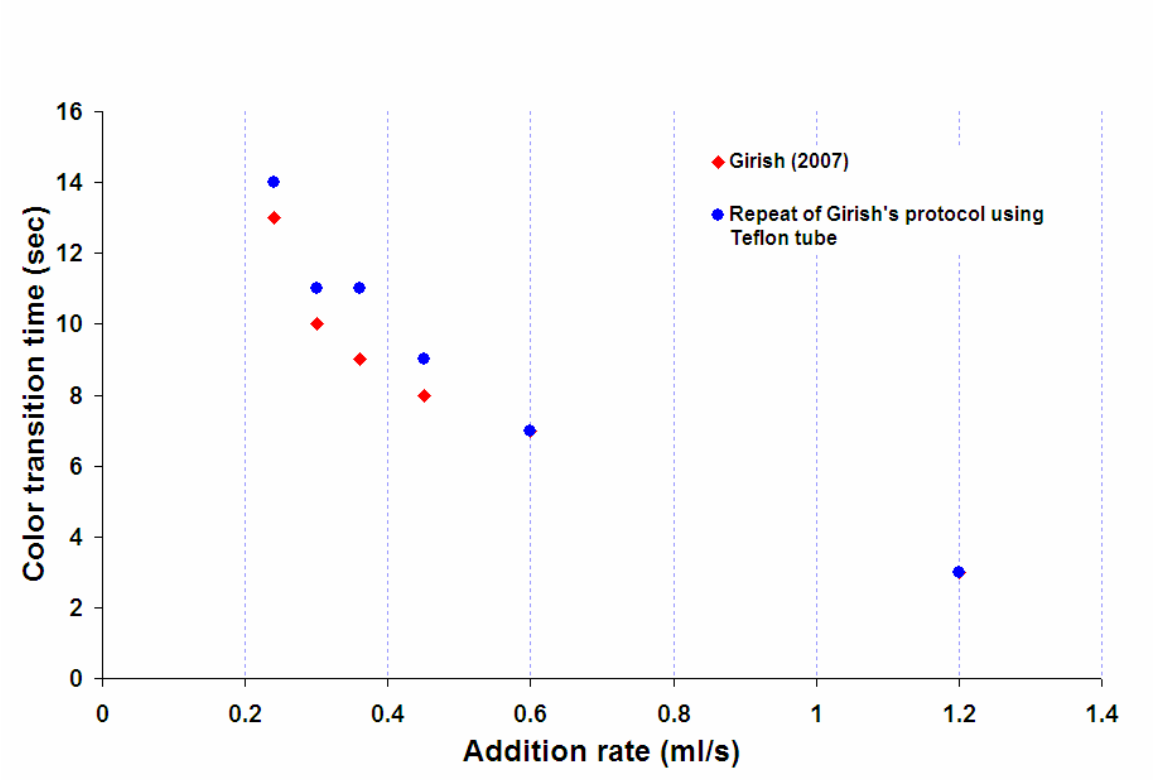

Figure 5.12: Effect of addition rate on color transition time at 30^0 C. Synthesis conditions: [$HAuCl_4$]: 0.05 M; [N_2H_5OH]: 0.5 M; [AOT]: 0.2 M; [Brij 52]: 0.1 M; [water]/ [AOT]: 8.

5.6 Conclusions

It was found that the unreacted gold chloride peak observed in UV-visible spectroscopy is due to the unavailability of sufficient hydrazine to completely reduce gold chloride, which is due to the incompatibility of hydrazine hydrate with the new PVC tube previously used. Stability of gold nanoparticles synthesized increased with increase in the hydrazine concentration. Increase in hydrazine concentration results in increase of reaction mixture pH, which affects stability. Changing pH of gold chloride slowed down the agglomeration process. Changing the pH of gold chloride to 8 decreases its reactivity and hence slows down the process. The trend in nanoparticle size and color transition time with the addition rate matched fairly well with the trend reported previously.

5.7 References

1. M. Girish, 'Nanoparticle synthesis in microemulsions', Master of Engineering Report, *Indian Institute of Science,* 2007.
2. C. L. Chiang, 'Controlled growth of gold nanoparticles in AOT/$C_{12}E_4$/Isooctane mixed reverse micelles', *Journal of Colloid and Interface Science,* 239, 2001, 334–341.
3. http://www.gasdetection.com/TECH/hydrazine.html accessed on 11/13/2007.
4. N. N. Greenwood and A. Earnshaw, 'Chemistry of the elements', Butterworth-Heinemann publication, 1997.
5. M. G. Spirin, S. B. Brichkin, and V. F. Razumov, 'Synthesis and Stabilization of Gold Nanoparticles in Reverse Micelles of Aerosol OT and Triton X-100' *Colloid Journal,* 67, 2005, 485-490.
6. X. Ji, X. Song, J. Li, Y. Bai, W. Yang, and X. Peng, 'Size control of gold nanocrystals in citrate reduction: The third role of citrate', *Journal of American Chemical Society*, 129, 2007, 13939-13948.
7. A. I. Bulavchenko, A. T. Arymbaeva, O. A. Bulavchenko, V. V. Tatarchuk, and N. I. Petrova, 'The preparation of gold nanoparticles in Triton N-42 reverse micelles after preliminary concentration of from acid sulfate-chloride solutions', *Russian Journal of Physical Chemistry*, 80, 2006, 1980-1985.
8. S. Chatterjee, R. K. Mitra, B. K. Paul, and S. C. Bhattacharya, 'Interface of AOT/Brij mixed reverse micellar systems: Conductometric and spectrophotometric investigations', *Journal of Colloid and Interface Science*, 298, 2006, 935-941.
9. L. M. Liz-Marzan, 'Nanoscale Materials', Kluwer academic publishers 2004.

Chapter 6

Synthesis of FePt nanoparticles in microemulsions

FePt nanoparticles have gained lot of attention as they have potential applications in ultra high density magnetic media. The coercivity or the magnetic anisotropy energy is an important property, which determines the stability of the magnetization in bulk material as well as in nanoparticles. This coercive force should be higher for the materials to be useful in high density magnetic data storage. This coercivity depends on various factors such as size (for metals), size and composition (for alloys) and various forms of anisotropy. Face centered tetragonal (FCT) structured FePt alloys have large magnetocrystalline anisotropy (K_u = 6.6-10 × 10^6 J/m^3) and good chemical stability [1], which makes them ideal candidates for high density storage applications. Synthesizing FePt nanoparticles with precise control over their size, size distribution and composition will be the main objective for any synthesis method. Microemulsion based synthesis has the capability to achieve good control over the size and composition.

6.1 Synthesis of FePt nanoparticles

FePt nanoparticles are synthesized based on the protocol developed by Ramanath et al. [2]. Ramanath et al. have synthesized FePt nanoparticles in microemulsions stabilized by nonionic surfactants Brij 52 and Brij 56 in isooctane. Initial experiments were performed following the protocol reported except that no co-surfactant was used in these experiments. Water to surfactant ratio of 1.42 was used. Metal salt microemulsion consists of 1:1 molar ratio of metal salts ($FeCl_3$ and K_2PtCl_4) dissolved in droplet aqueous cores. Hydrazine hydrate of appropriate concentration was added directly to the microemulsion at 30^0C. Rushton turbine impeller-Baffle system was used for efficient mixing of the solutions. Impeller was

operated at 750 ± 20 rpm. But initial experiments didn't yield FePt nanoparticles and no color change was observed upon adding hydrazine contrary to what was reported [2]. This may be due to the fact that the metal salt concentrations used were very low. When the metal salt concentrations were increased to 0.25 M, a color change (from yellow color of metal salts to the dark brown of FePt nanoparticles) was observed. DLS showed the presence of bigger size clusters of size 250-300 nm.

Addition of 1-butanol has decreased the hydrodynamic diameter to 110-120 nm. UV-visible absorption spectrum of FePt nanoparticles is shown in Figure 6.1.

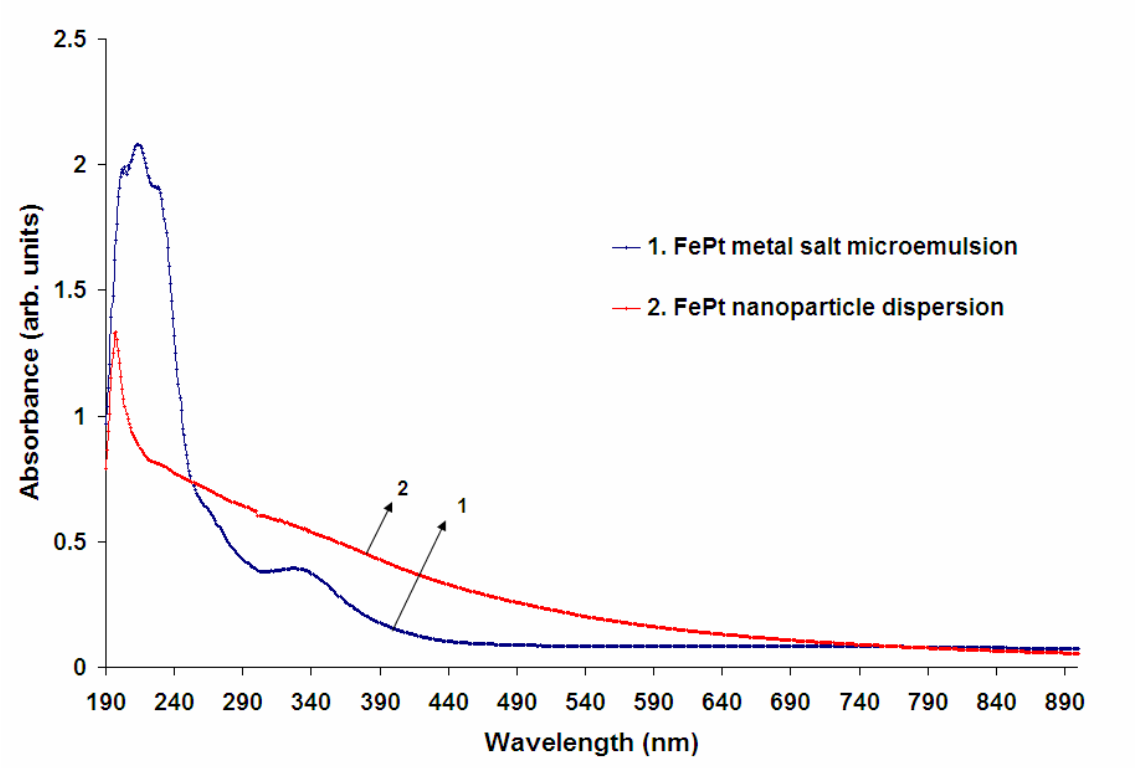

Figure 6.1: UV-Visible absorption spectrum of FePt metal salt microemulsion and FePt nanoparticle dispersion. Synthesis conditions: [$FeCl_3$]: 0.25 M; [K_2PtCl_4] = 0.25 M; [Brij 52]: 1.16 M, 1-Butanol: 3mmol; [water]/ [Brij 52]: 1.42. 1.25 ml of Hydrazine hydrate was added directly to the microemulsion.

The FePt nanoparticles synthesized were characterized by XRD. The x-ray diffractogram of the sample is shown in Figure 6.2.

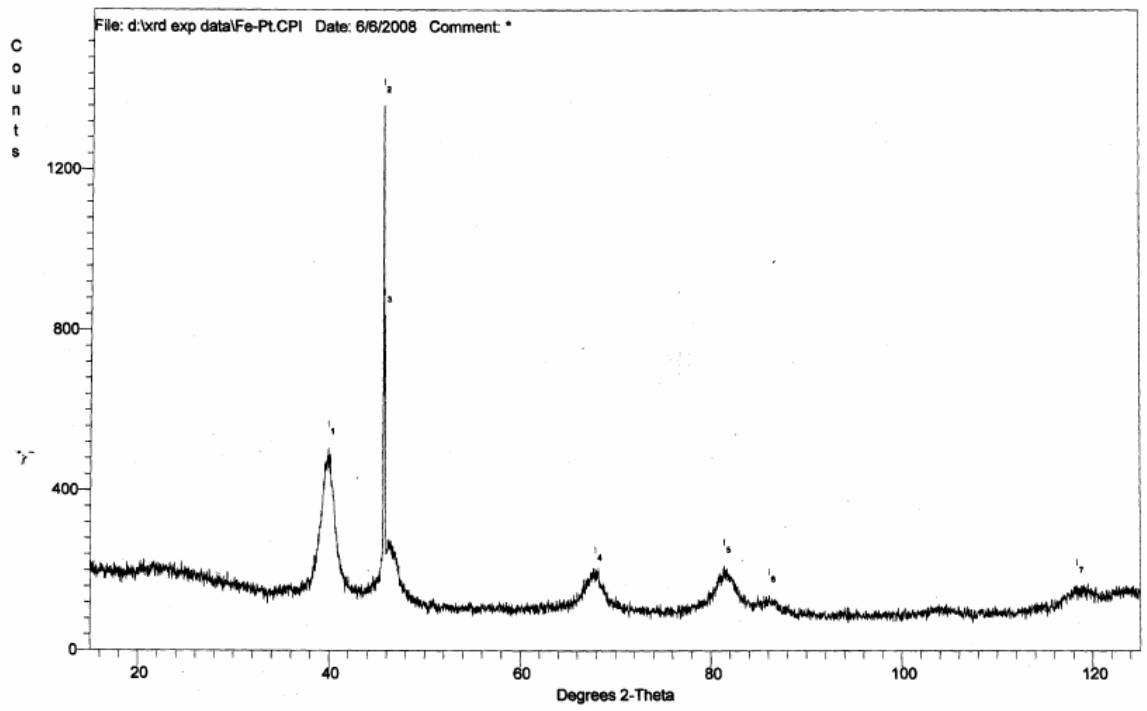

Figure 6.2: X-ray diffractogram of FePt nanoparticles. Synthesis conditions: [$FeCl_3$]: 0.25 M; [K_2PtCl_4] = 0.25 M; [Brij 52]: 1.16 M, 1-Butanol: 5 mmol; [water]/ [Brij 52]: 1.42. 1.25 ml of Hydrazine hydrate was added directly to the microemulsion.

The above XRD pattern was compared with the reported XRD pattern of face centered cubic (FCC) structured FePt alloy (1997 JCPDS 29-0717 – International Centre for Diffraction Data) and this comparison revealed that the FePt nanoparticles synthesized are alloys having FCC structure. The crystallite size estimated from peak width using the Debye-Scherrer formula is 8.5 nm.

6.2 Conclusions

FePt nanoparticles were synthesized in water/Brij 52/isooctane microemulsions based on the protocol reported by Ramanath et al. The concentrations of metal salts used were higher than the values reported. DLS showed the presence of bigger size clusters. The absorption peaks of metal salts disappeared after reduction. XRD pattern showed that the synthesized FePt nanoparticles are alloys having FCC structure. The crystallite size estimated from XRD is 8.5 nm.

6.3 References

1. S. Sun, 'Recent Advances in Chemical Synthesis, Self-Assembly and Applications of FePt Nanoparticles' *Advanced Materials* 2006**,** 18, 393-403.
2. Q. Yan, A. Purkayastha, T. Kim, R. Kroger, A. Bose, and G. Ramanath, 'Synthesis and Assembly of Monodisperse High-Coercivity Silica-Capped FePt Nanomagnets of Tunable Size, Composition, and Thermal Stability from Microemulsions' *Advanced Materials.,*2006, 18, 2569-2573.

Chapter 7

Summary and recommendations

7.1 Summary

The main contributions of this project are summarized below

- The appearance of unreacted gold chloride peak in absorption spectra of the gold nanoparticle samples prepared using a PVC tube is attributed to a side reaction between the tube and reducing agent hydrazine hydrate as they are incompatible.
- The stability of the gold nanoparticle dispersions increases with increasing hydrazine hydrate concentration. Stable gold nanoparticles can be synthesized even at slower addition rates by using higher hydrazine concentrations.
- pH of the reaction mixture has an important role in stabilizing the gold nanoparticles synthesized using this protocol as the reactivity of both the reactants (gold chloride and hydrazine hydrate) is pH dependent.
- Changing the pH of gold chloride to eight slowed down the agglomeration process. TEM images showed the presence of clusters of small particles, which indicates the fact that the nanoparticles prepared are not properly stabilized.
- The trend observed in mean particle size and color transition time with addition rate for gold nanoparticles prepared using Teflon tube for injection matched the trend reported using an old (possibly reduced) PVC tube.
- There is no clear trend in the mean particle size with addition rate for gold nanoparticles prepared in water/AOT/Brij 52/isooctane mixed microemulsions.

- FePt nanoparticles were synthesized using higher concentrations of the metal salts and DLS showed presence of bigger size FePt nanoparticles (> 100 nm). The alloy nature of FePt nanoparticles is confirmed by XRD.

7.2 Recommendations for future work

- Injecting gold chloride microemulsion into hydrazine microemulsion may result in more monodisperse and stable nanoparticles.
- Gold nanoparticle formation in microemulsions should be studied using stopped flow reactor to understand the kinetics of the reaction.
- Concentrations of metal salts and surfactant used have to be varied to standardize the protocol to get smaller size (< 20 nm) monodisperse FePt alloy nanoparticles.
- Different molar ratios of [Fe]/ [Pt] need to be used to compare the ratio taken initially with the ratio present in nanoparticles.

Appendix: List of chemicals

S. No	Chemical name, Molecular formulae	Molecular weight (g/gmol)	Catalog No., Batch No.	Supplier	Grade
1	Chloroauric acid, $HAuCl_4.3H_2O$	393.83	254169, 11315TD	Aldrich	99.999%
2	Chloroauric acid, $HAuCl_4.3H_2O$	393.83	223620050, A0230907	Acros organics	99.999%
3	Hydrazine Hydrate N_2H_5OH	50.06	38502, E05A-1005-1404-13	S.D. Fine Chem.	99%
4	Dioctyl sulfosuccinate sodium salt, $C_{20}H_{37}O_7SNa$	444.55	D4422, 095K0203	Sigma	99%
5	Brij 30, $C_{12}H_{25}(OCH_2CH_2)_4OH$	362.0	P4391, 093K01091	Sigma	98%
6	Brij 52, $C_{16}H_{33}(OCH_2CH_2)_2OH$	330.0	388831, 03705DD	Aldrich	-
7	Isooctane, C_8H_{18}	114.26	604717100017 30	Merck	HPLC
8	Ferric Chloride, $FeCl_3$	162.20	451649	Aldrich	99.99%
9	Potassium tetrachloro platinate, K_2PtCl_4	415.11	323411, 00731AE	Aldrich	99.99%

Table A1: List of chemicals used in this study to synthesize gold and FePt nanoparticles in microemulsions